1 **The neuron-intrinsic membrane skeleton is required for motor neuron integrity**

2 **throughout lifespan**

3

4 Carrie Ann Davison[1], Daniela Garcia[2], Chengye Feng[1], Hongyan Hao[2], Erik M. Jorgensen[3,4],

5 Marc Hammarlund[1,2,5]

6

7 [1]Department of Genetics, Yale University School of Medicine, New Haven, CT, USA

8 [2]Department of Neuroscience, Yale University School of Medicine, New Haven, CT, USA

9 [3]School of Biological Sciences, University of Utah, Salt Lake City, UT, USA

10 [4]Howard Hughes Medical Institute, Salt Lake City, UT, USA

11 [5]Lead Contact

12

13 Correspondence: marc.hammarlund@yale.edu

14

Abstract

Axons experience physical stress throughout an organism's lifetime, and disruptions in axonal integrity are hallmarks of both neurodegenerative diseases and traumatic injuries. The spectrin-based membrane periodic skeleton (MPS) is proposed to have a crucial role in maintaining axonal strength, flexibility, and resilience. To investigate the importance of the intrinsic MPS for GABAergic motor neuron integrity in *C. elegans*, we employed the auxin-inducible degron system to degrade β-spectrin/UNC-70 in a cell-type specific and time-dependent manner. Degradation of β-spectrin from all neurons beginning at larval development resulted in widespread axon breakage and regeneration in VD/DD GABAergic motor neurons in both larval and adult animals. Similarly, targeted degradation of β-spectrin in GABA neurons alone resulted in extensive breakage. Moreover, we found that depleting β-spectrin from the mature nervous system also induced axon breaks. By contrast, epidermal β-spectrin was not required for axon integrity of VD/DD neurons. These findings demonstrate the cell-intrinsic importance of neuronal β-spectrin/UNC-70 for axon integrity both during development and in adulthood.

Introduction

Throughout the lifetime of an organism, neurons are subject to physical stress. Traumatic injury can disrupt axon integrity; even without trauma, axons must maintain resilience for the life of the neuron. The spectrin-based membrane periodic skeleton (MPS) has emerged as a key support for axon integrity. The MPS is a lattice framework of actin rings connected by spectrin tetramers (D'Este et al., 2015; He et al., 2016; Xu et al., 2013) that is proposed to provide mechanical resistance and flexibility to neurites under physiological strain (Hammarlund et al., 2007; Krieg et al., 2014). In axons, the MPS exhibits a periodicity of approximately 190 nm (D'Este et al., 2015; He et al., 2016; Xu et al., 2013), and this periodicity is important for proper neuronal function including regulating axon diameter and conduction (Costa et al., 2020), organizing discrete membrane domains (C. Zhang et al., 2013), regulating endocytosis in the axon-initial segment (Wernert et al., 2024), promoting axonal transport (Jia et al., 2019; Lorenzo et al., 2019), and limiting tension propagation to enable localized signaling (Català-Castro et al., 2025). Disruptions in the MPS cause axon degeneration in *C. elegans* (Hammarlund et al., 2007; Krieg et al., 2014, 2017), *Drosophila* (Hülsmeier et al., 2007; Lorenzo et al., 2010), and mice (Huang, Zhang, Ho, et al., 2017; Liu et al., 2020; Lorenzo et al., 2019). In humans, mutations in α and β spectrin cause a variety of neurological disorders including spinocerebellar ataxia type 5 (Ikeda et al., 2006), early infantile epileptic encephalopathy-5, as well as other forms of developmental delay and intellectual disability (reviewed in (Lorenzo et al., 2023)). A deeper understanding of the function of the MPS within neurons is crucial for advancing nervous system resilience in injury and disease.

Spectrin tetramers consist of two α and two β subunits each containing multiple spectrin repeat domains that fold into three-helix bundles (Speicher & Marchesi, 1984; Yan et al., 1993). These bundles can reversibly unfold to act as spring-like "shock absorbers" and buffer tension in axons (Dubey et al., 2020). While humans have two α-spectrins and five β-spectrins, invertebrates

55   have only one of each. In *C. elegans*, the sole β-spectrin is encoded by *unc-70* (Hammarlund et

56   al., 2000); for simplicity, we will typically refer to this protein simply as β-spectrin.

57   β-spectrin has been proposed to provide tension and mechanical resistance to axons

58   (Hammarlund et al., 2007; Krieg et al., 2014, 2017). Loss of β-spectrin causes spontaneous

59   breakage of sensory and motor neurons due to the mechanical stress of body movement

60   (Hammarlund et al., 2007; Krieg et al., 2014). Some evidence suggests this is due to a cell-

61   intrinsic function for the spectrin cytoskeleton. For example, GABA neurons express β-spectrin

62   (Taylor et al., 2021), and the endogenously tagged MPS has been visualized in *C. elegans*

63   neurons (Glomb et al., 2023; He et al., 2016; Krieg et al., 2017), consistent with MPS function in

64   neurons. Further, cultured *C. elegans* touch neurons have reduced apparent membrane tension

65   in the absence of β-spectrin, indicating that loss of β-spectrin alters the cell-intrinsic properties of

66   the neuron (Krieg et al., 2014).

67   However, β-spectrin is also expressed in other tissues including the epidermal tissues

68   surrounding neurons, (Coakley et al., 2022; C. Wang et al., 2020; White et al., 1997). The

69   importance of the spectrin cytoskeleton in surrounding tissues for axon function and integrity has

70   been increasingly appreciated. For example, in mammals, loss of αII and βII spectrin in Schwann

71   cells disrupts myelination of peripheral nervous system (PNS) axons (Susuki et al., 2011), and

72   loss of glial βII-spectrin disrupts paranode formation and maintenance (Susuki et al., 2018). In *C.*

73   *elegans,* epidermal β-spectrin has been shown to contribute to the axon integrity of touch receptor

74   neurons (TRNs) (Bonacossa-Pereira et al., 2022; Coakley et al., 2020, 2022; Das et al., 2021;

75   Krieg et al., 2014, 2017). The TRNs are embedded within the epidermis (Chalfie & Sulston, 1981),

76   and the attachment between the neuron and epidermis has been shown to protect axons from

77   movement-induced damage (Bonacossa-Pereira et al., 2022; Coakley et al., 2020).

78   Whether the spectrin cytoskeleton acts in neurons or in associated tissue to preserve axon

79   integrity in neuron types that are not embedded in skin is unclear. The *C. elegans* DD and VD

80   GABA neurons extend commissural axons that contact the skin, but are not embedded in it

81   (Sulston & Brenner, 1997; White et al., 1997). β-spectrin in both muscle and the epidermis has

82   been shown to induce DD/VD axon defects in response to hypergravity (Kalichamy et al., 2020).

83   Furthermore, it has been reported that loss of β-spectrin from the epidermis results in breakage

84   of DD/VD axon commissures, while loss from neurons has no effect (Coakley et al., 2022). On

85   the other hand, a neuron-intrinsic function remains a compelling hypothesis based on the

86   structure of the MPS (Xu et al., 2013) and on data from neurons in culture (Das et al., 2021; Dubey

87   et al., 2020; Krieg et al., 2014). Some previous studies investigating the importance of β-spectrin

88   for the integrity of the DD and VD GABA neurons have used full body mutations in *unc-70,* and

89   did not fully address the question of the relative contribution of intrinsic and extrinsic spectrin to

90   axon integrity (Hammarlund et al., 2007; Kalichamy et al., 2020). Thus, the importance of intrinsic

91   and extrinsic spectrin for axon integrity in DD and VD GABA neurons remains unclear.

92   To characterize the importance of the intrinsic spectrin cytoskeleton for the integrity of

93   GABA neurons in *C. elegans,* we used the auxin-inducible degron (AID) system (Ashley et al.,

94   2021; L. Zhang et al., 2015) to degrade β-spectrin in a cell-specific and time-dependent manner.

95   Degradation of β-spectrin from all neurons resulted in the widespread breakage of the DD and

96   VD GABA neuron commissures. When the ability of axons to regenerate was inhibited, large

97   portions of the dorsal nerve cord degenerated. By contrast, degradation of β-spectrin from the

98   epidermis did not affect GABA neuron integrity. We also find that loss of β-spectrin from the

99   epidermis does not affect the ability of axons to regenerate after laser axotomy. Together, these

100   results demonstrate the cell-intrinsic importance of β-spectrin for axon integrity and establish

101   targeted degradation of neuronal β-spectrin as a tool to study mechanisms of axon regeneration

102   and degeneration.

103

104 **Results**

105 **A system to acutely deplete β-spectrin and the spectrin-based membrane skeleton**

106   To determine which tissues require β-spectrin to maintain GABA neuron integrity, we used

107 targeted protein degradation (Ashley et al., 2021; L. Zhang et al., 2015) to specifically deplete β-

108 spectrin from designated tissues in an otherwise wild-type background. We used an allele of *unc-*

109 *70/*β-spectrin in which a small degron tag has been inserted into the endogenous *unc-70/*β-

110 spectrin gene by CRISPR (UNC-70::AID) (Glomb et al., 2023) (Figure S1). We then expressed

111 the E3 ligase TIR1 from *Arabidopsis thaliana* (atTIR1) under the pan-neuronal promoter *Prab-3*.

112 Upon the addition of 1mM Auxin, atTIR1 will bind the degron tag resulting in rapid

113 polyubiquitylation and proteasomal degradation (Holland et al., 2012; L. Zhang et al., 2015) of β-

114 spectrin in all neurons. This allele has previously been used successfully to rapidly and reversibly

115 degrade β-spectrin from the DA9 neuron (Glomb et al., 2023). Importantly, in the absence of

116 auxin, the movement of the animals is normal, indicating that neither the degron tag on β-spectrin

117 nor expression of atTIR1 perturb neuronal morphology or function (Figure 1A).

118   We allowed young adults to lay eggs on NGM plates containing 1mM natural auxin indole-

119 3-acetic acid (IAA) for two hours. Newly hatched larvae are thus immediately exposed to auxin,

120 allowing for pan-neuronal degradation of β-spectrin from the L1 larval stage (L1:β-

121 spectrinΔneurons). (The eggshell has low permeability to IAA, therefore efficient degradation in

122 the embryo is not expected (Negishi et al., 2019; L. Zhang et al., 2015)). We assessed these L1:β-

123 spectrinΔneurons animals at the L4 stage and found that they exhibit abnormal body posture,

124 reduced body length, and delayed development (Figure 1B-E).

125   To directly assess the effect of L1:β-spectrinΔneurons on the spectrin-based membrane

126 skeleton (MPS), we imaged SPC-1/α-spectrin in GABA neurons, using an endogenously tagged

127 split-GFP allele (Jia et al., 2019). In the MPS, α-spectrin and β-spectrin obligate dimers assemble

128 into tetramers (Speicher & Marchesi, 1984; Yan et al., 1993). Expression levels of β-spectrin have

6

129   been shown to affect expression of α-spectrin in *Drosophila* (Hülsmeier et al., 2007)*.* Furthermore,

130   it was previously shown that auxin-inducible degradation of β-spectrin results in eradication of the

131   axonal MPS and loss of α-spectrin from axons of DA9 neurons (Glomb et al., 2023). Thus, axonal

132   α-spectrin can be used as an endogenous marker for the presence of β-spectrin and an intact

133   MPS.

134   We assessed L1:β-spectrinΔneurons animals 24 hours after egg lay, at which time both

135   control and L1:β-spectrinΔneurons animals are still in the L1 larval stage. We found that α-spectrin

136   was robustly localized in axons of GABA neurons in control animals (of the same genotype, but

137   without auxin) (Figure 2B). (We would not expect to observe the periodic nature of the MPS under

138   our imaging conditions due to resolution constraints.) However, in the presence of auxin, α-

139   spectrin was absent from the axons of DD GABA neurons (Figure 2B,C). At this early larval

140   timepoint, VD axon outgrowth had not yet occurred and therefore the MPS in VD axons could not

141   be assessed. These data indicate that β-spectrin is rapidly degraded, disrupting the MPS and

142   resulting in loss of α-spectrin from GABA neuron axons. Interestingly, we also observed

143   accumulation of α-spectrin in the cell bodies of GABA neurons (Figure 2B, S2A,B) (see

144   Discussion).

145   **Axons break when neurons lack β-spectrin**

146   To determine whether L1:β-spectrinΔneurons result in axon breaks, we visualized the

147   VD/DD neurons at the L4 stage in animals raised on auxin. We found degradation of β-spectrin

148   from all neurons resulted in widespread breakage of GABA neuron axons (Figure 3B-C). The

149   axons of VD and DD-type GABA neurons typically overlap in the dorsal and ventral nerve cord,

150   but their commissures are typically non-overlapping. Nearly 60% of axons were broken at larval

151   stage L4, and 80% of animals exhibited gaps in the dorsal nerve cord (Figure 3B-D). Formation

152   of the DD GABA neurons occurs embryonically before UNC-70 is degraded. By contrast, the VD

153   GABA neurons are born post-embryonically and complete axon outgrowth by the L2 larval stage.

154   To confirm that the phenotype is caused by axon breakage rather than axon outgrowth defect, we

155   quantified the percentage of broken axons (Figure 3E) and number of visible intact VD/DD

156   neuronal commissures (Figure 3F) at the L2 stage. At the L2 stage, when development is

157   complete, nearly all commissures are intact (Figure 3E). By contrast, at L4 stage, most

158   commissures are broken (Figure 3C). While there is a decrease in the number of intact

159   commissures in L1:β-spectrinΔneurons at the L2 stage compared with control, this is likely due to

160   spontaneous breakage shortly after or even during outgrowth (Figure 3F). This analysis reveals

161   that loss of neuronal β-spectrin has minimal effect on outgrowth of the GABA neurons, but instead

162   results in hyper-fragile axons that progressively break, consistent with previous results

163   (Hammarlund et al., 2007).

164   Degradation of neuronal β-spectrin resulted in robust regeneration of the GABA axons

165   with many broken axons exhibiting growth cones (Figure 3B, S3B). This indicates that many

166   axons that break also successfully regenerate (Hammarlund et al., 2007), complicating an

167   accurate quantification of total axon breakage. To determine the full extent of axon breakage upon

168   β-spectrin degradation, we introduced a mutation in the kinase *dlk-1* to prevent axon regeneration

169   (Hammarlund et al., 2009). Loss of *dlk-1* together with L1:β-spectrinΔneurons revealed that 94%

170   of axons break (Figure 3H, I) and 100% of animals have gaps in their dorsal nerve cord by the L4

171   stage (Figure 3J). In most animals, large portions of the dorsal nerve cord were fully degenerated

172   (Figure 3H). Consistent with our observations for L1:β-spectrinΔneurons animals, *dlk-1;* L1:β-

173   spectrinΔneurons animals were small (Figure 3H) and did not have large defects in GABA neuron

174   outgrowth (Figure 3K,L). The phenotype of *dlk-1;* L1:β-spectrinΔneurons animals was consistent

175   whether a genetic loss of function in *dlk-1* or a small molecular inhibitor of DLK-1 (GNE-3511)

176   was used (Figure S3C,D). Thus, neuronal β-spectrin is essential for GABA neuron integrity, and

177   loss of DLK-1 provides an improved way to quantify breakage.

178   **β-spectrin in the skin is not required for GABA neuron integrity or regeneration**

179   Recently, epidermal β-spectrin has been proposed to protect touch receptor neurons

180   (TRNs) and GABA neurons from breakage and degeneration (Coakley et al., 2022). Both TRNs

181   and GABA motor neurons make close contacts with the epidermis. However, while the TRNs are

182   embedded within the skin, the GABA neurons are not. To investigate the role of epidermal β-

183   spectrin for GABA neuron integrity, we degraded β-spectrin from the epidermis using a variety of

184   epidermal promoters (P_{col-10}:atTIR1 or P_{dpy-7}::atTIR1 and P_{col-19}:atTIR1) (L1:β-spectrinΔskin) and

185   confirmed degradation of epidermal β-spectrin was successful by observing disrupted epidermal

186   α-spectrin (Figure S4). We observed no axonal breakage in L1:β-spectrinΔskin animals at the L4

187   stage (Figure 4A, B, D). To assess if axons had broken and regenerated, we used an inhibitor of

188   DLK-1 (DLKi) to prevent regeneration. We observed only 2% of axons broken in L1:β-

189   spectrinΔskin + DLKi animals (Figure 4B) in contrast to 98% in L1:β-spectrinΔneurons + DLKi

190   animals at the L4 stage (Figure S3C). In a low proportion of animals we observed small gaps in

191   the dorsal nerve cord when β-spectrin was degraded using the *col-10* promoter (24% of animals)

192   (Figure 4A,C) or using the *dpy-7* and *col-19* promoters (8% of animals) (Figure 4E). This breakage

193   was not exacerbated by inhibition of DLK-1 (Figure 4C). We hypothesize that these gaps are due

194   to instability at the axon tips, rather than breakage along the axon shaft (see Discussion).

195   To investigate if epidermal spectrin plays additional roles in integrity or regrowth of motor

196   neurons in the context of injury, we performed laser axotomy on the VD GABA neurons in L1:β-

197   spectrinΔskin animals. Spectrin has been shown to regulate axon-glia attachments (Garcia-

198   Fresco et al., 2006; Susuki et al., 2011, 2018) important for neuronal integrity, and β-spectrin

199   regulates the attachment of touch receptor neurons to the epidermis (Coakley et al., 2020). The

200   extracellular environment is known to affect the ability of VD/DD axons to regenerate after injury

201   (Edwards & Hammarlund, 2014), and a previous report has visualized epidermal α-spectrin

202   localized to regrowing PLM touch receptor neurons after injury (Coakley et al., 2022). Thus, it is

203   possible that epidermal spectrin may influence VD axon regrowth after injury through either direct

204 physical scaffolding or changes in the extracellular environment. However, L1:β-spectrinΔskin

205 animals did not have a defect in the ability of axons to regrow after injury (Figure 4F). Together,

206 these results demonstrate that epidermal β-spectrin does not have a large effect on GABA neuron

207 integrity in basal or injury conditions.

Cholinergic neurons, but not skin, modulate the effect of GABA neuron spectrin loss

209 We next sought to determine if loss of β-spectrin only from GABA neurons caused similar

210 breakage to pan-neuronal degradation. We used the GABA-specific *unc-47* promoter to drive

211 expression of atTIR1, and the *dlk-1* mutant background to block regeneration and allow accurate

212 quantitation. Interestingly, loss of β-spectrin only from GABA neurons (L1:β-spectrinΔGABA)

213 resulted in 100% of animals with degeneration in their dorsal nerve cord (Figure 5A,C) but only

214 approximately 50% of axons broken at the L4 stage (Figure 5B). Multiple atTIR1 arrays gave

215 similar phenotypes (Figure S5A), and α-spectrin distribution was disrupted in all GABA

216 commissures regardless of axon breakage (Figure S5B,C). Thus, loss of β-spectrin from GABA

217 neurons is sufficient to cause axon breakage, but breakage is enhanced when β-spectrin is lost

218 from all neurons.

219 To further explore how loss of GABA spectrin might be enhanced by loss of spectrin from

220 other tissues, we degraded β-spectrin from GABA neurons in combination with two other tissues:

221 the skin or the cholinergic neurons. Degradation of β-spectrin from both GABA neurons and the

222 skin did not exacerbate breakage when compared to GABA alone (Figure 5B). However,

223 degradation from both GABA and cholinergic neurons resulted in 83% of axons broken, similar to

224 that observed with pan-neuronal degradation (Figure 5B).

225 How might loss of β-spectrin from cholinergic neurons enhance axon breakage in GABA

226 neurons that also lack β-spectrin? We considered the possibility that the cholinergic neurons

227 might physically scaffold the GABA neurons. Cholinergic motor neurons such as VA and VB also

228 extend commissures across the body of the worm, and these axons can fasciculate with GABA

229 neuron axons. In this model, the elimination of β-spectrin only in GABA neurons might have a

230 weaker effect because undamaged cholinergic neurons are available as scaffolds. To test this

231 model, we visualized the cholinergic neuron commissures in L1:β-spectrinΔGABA animals using

232 the pan-cholinergic marker P_{unc-17}::TagRFP or P_{unc-17}::mTagBFP2 (Figure S5D,F). We found that

233 fasciculation events are rare, with only 1-2 of the 19 GABA commissures in each animal

234 fasciculated with a cholinergic commissure. Thus, the scaffolding model cannot explain the

235 approximately 8 unbroken commissures per animal when spectrin is lost from only GABA

236 neurons. While we observed the majority of fasciculated GABA commissures are intact, which

237 suggests a possible correlation between fasciculation and preventing breakage (Figure S5D,E),

238 we also observed fasciculated GABA commissures that had broken (Figure S5E, F). Therefore,

239 fasciculation is not sufficient to prevent breakage of GABA neurons caused by degradation of β-

240 spectrin. Together, these results indicate that scaffolding by fasciculation may inhibit axon

241 breakage but is not the primary way that β-spectrin in cholinergic neurons acts to limit breakage

242 in GABA neurons.

243 Next, we considered the possibility that differences in movement might underlie the role

244 of cholinergic β -spectrin in GABA neuron breakage. Degradation of β-spectrin from only GABA

245 neurons resulted in a mild movement phenotype (data not shown) and no significant effect on

246 body size (Figure 5D,E). In contrast, degradation of β-spectrin from both GABA and cholinergic

247 neurons reduced body size and strongly affected movement (Figure 5D,E). These animals are

248 hyper-curled, similar to β-spectrinΔneurons animals (Figure 5D). We hypothesize the increased

249 breakage in β-spectrinΔneurons and β-spectrinΔGABAΔcholinergic animals is due to increased

250 physical strain on the GABA neurons resulting from altered body movement and posture. This is

251 consistent with previous results showing that the strain of movement induces breakage in hyper-

252 fragile axons (Hammarlund et al., 2007).

253 **Spectrin is required in mature neurons to prevent axon breaks.**

254   Although there have been multiple reports of axon damage due to loss of β-spectrin

255   (Coakley et al., 2020, 2022; Hammarlund et al., 2007; Krieg et al., 2014, 2017), in general, these

256   studies relied on constitutive loss of β-spectrin. In the above experiments, we exposed animals

257   to auxin at the L1 stage, triggering β-spectrin degradation while the nervous system is still

258   developing. In particular, the VD GABA neurons are still extending growth cones at this stage,

259   while the DD GABA neurons still must undergo extensive synaptic remodeling (Hallam & Jin,

260   1998; White et al., 1978). We next examined whether acute loss of β-spectrin in mature neurons

261   is sufficient to cause axon breakage. We exposed β-spectrinΔneurons animals to auxin at the L4

262   stage, at which time the GABA neurons are fully mature. After 48 hours, approximately 50% of

263   VD/DD axons were broken, with the majority exhibiting evidence of regrowth, including large

264   growth cones (Figure 6A, C). Thus, like developing neurons, mature neurons depend on intrinsic

265   neuronal β-spectrin to preserve axon integrity.

Axon breakage is delayed following neuronal spectrin disruption

267   Finally, we investigated the temporal relationship between loss of the MPS and axon

268   breakage. We degraded β-spectrin for 24 or 48 hours in both the developing and mature nervous

269   system. In both developing and mature neurons, α-spectrin distribution was completely disrupted

270   within 24 hours of auxin treatment, indicating that AID activation rapidly degrades β-spectrin and

271   disrupts the MPS (Figure 2, Figure 6). Strikingly, however, breakage was not observed at 24

272   hours, but was robust at 48 hours (Figure S2C, S3C, 6C). For example, in L1:β-spectrinΔneurons

273   animals 24 hours after egg lay onto auxin plates, α-spectrin distribution was disrupted (Figure 2);

274   however, we found no visible breakage of the DD neurons (at this timepoint the VD axons had

275   not yet developed) (Figure S2C). After 48 hours of auxin treatment, L1:β-spectrinΔneurons

276   animals exhibit widespread breakage (Figure 3, S3). Similarly, in the mature nervous system, L4

277   animals exposed to auxin for 24 hours had significantly disrupted α-spectrin (Figure 6A, S6A),

278   and while axon morphology was abnormal including large swellings and thinnings (Figure 6A,B),

279 axons were continuous and not visibly broken. By 48 hours, approximately half of all axons were

280 visibly broken (Figure 6A,C). As in the larval stage animals, we also observed α-spectrin

281 accumulation in the cell bodies when β-spectrin is degraded (Figure S6B,C). Therefore, in both

282 the developing and mature nervous systems, MPS disruption significantly precedes axon

283 breakage.

284

285

286 **Discussion**

287 **The neuron-intrinsic spectrin cytoskeleton is required for motor neuron axon integrity**

288 **during typical and atypical movement**

289 We have shown that the intrinsic MPS is required for VD/DD GABAergic motor neuron

290 integrity in *C. elegans*. Degradation of β-spectrin during development and in the mature nervous

291 system altered α-spectrin distribution and resulted in breakage of VD/DD commissures. We

292 observed α-spectrin accumulated in the cell bodies when β-spectrin was degraded. This is

293 consistent with previous observations in DA9 (Glomb et al., 2023). Without β-spectrin, α-spectrin

294 fails to be properly localized in the axon, remains highly mobile (Glomb et al., 2023), and the MPS

295 cannot be formed. Interestingly, degradation of β-spectrin only from GABA neurons resulted in

296 less breakage than degradation from all neurons or degradation from both GABA and cholinergic

297 neurons. We hypothesize this is due to more stressful body posture and movement when β-

298 spectrin is degraded from cholinergic neurons. Previous work has shown that the DVA neuron is

299 activated during compressive stress caused by body bending, and cell intrinsic loss of *unc-70*

300 using the Cre-lox system from the DVA neuron alone caused an "exaggerated" body posture

301 characterized by deeper body bends (Das et al., 2021). Similar body posture was observed in

302 both β-spectrinΔneurons and β-spectrinΔGABAΔcholinergic animals (Figure 5D). These deep

303 body bends may place additional stress on VD/DD axons, particularly where the commissures

304   squeeze between the muscle and the skin (Knobel et al., 1999), resulting in increased frequency

305   of breakage in neurons that lack β-spectrin. Overall, our data demonstrate that intrinsic β-spectrin

306   is required during both normal movement and stressful movement to maintain motor neuron axon

307   integrity.

Neuronal rather than epidermal spectrin protects GABA neurons from breakage

309   The importance of the intrinsic MPS has been shown across model organisms. Loss of

310   αII-spectrin from CNS neurons in mice causes widespread neurodegeneration and seizures

311   (Huang, Zhang, Ho, et al., 2017), and mice lacking αII-spectrin in the PNS have disrupted nodes

312   of Ranvier, mislocalized Kv1 K+ channels, degeneration of large-diameter myelinated axons, and

313   severe ataxia (Huang, Zhang, Zollinger, et al., 2017). Mathematical modeling describes how

314   spectrin tetramers within the MPS may provide mechanical neuroprotection through reversibly

315   unfolding to act as "shock absorbers" and buffer tension (Dubey et al., 2020). In *C. elegans*, the

316   MPS is under continuous tension in living neurons, and if this tension is disrupted by mutations in

317   β-spectrin, touch sensation is impaired (Krieg et al., 2014). Neurons in culture withstand

318   compression, torsion, and stretch through tension provided by the MPS and stiffness provided by

319   the microtubule cytoskeleton (Krieg et al., 2017). However, the importance of the intrinsic MPS

320   for axon integrity in *C. elegans* may vary by neuron type, morphology, and environment. Loss of

321   β-spectrin from DVA only causes axon buckling, not breakage or degeneration (Das et al., 2021).

322   Touch receptor neurons buckle in β-spectrin mutants, and while expression of epidermal β-

323   spectrin can decrease buckling, it does not rescue touch response, supporting the importance of

324   the intrinsic MPS for neuronal function (Krieg et al., 2014).

325   The *C. elegans* system offers numerous advantages for studying the importance of both

326   the intrinsic MPS and spectrin in surrounding tissues for neuronal function and integrity in a free-

327   living intact organism. Both TRNs (including the PLM neuron) and VD/DD GABAergic motor

328   neurons are in contact with the epidermis. The epidermis serves a glial-like function including

14

329   clearance of axonal fragments after injury and mediating communication with the extracellular

330   environment (reviewed in (Chisholm & Xu, 2012)). A spectrin scaffold within the epidermis has

331   also been shown to protect the integrity of TRNs, which are embedded in the epidermis and

332   mediate response to touch (Bonacossa-Pereira et al., 2022; Coakley et al., 2020, 2022). While

333   VD/DD axons are not embedded in the epidermis, they are in close contact with both the

334   epidermis and muscle. In a hypergravity-induced model of axon damage, epidermal and muscle

335   β-spectrin and the hemidesmosomes connecting axons to the epidermis promote GABAergic

336   motor neuron axon defects that occur most frequently along larger muscle cells (Kalichamy et al.,

337   2020). There it is possible that scaffolding and attachment to the epidermis may support VD/DD

338   axon integrity.

339   To test the contribution of epidermal β-spectrin for GABA neuron integrity, we degraded

340   epidermal β-spectrin using a variety of epidermal promoters (P_{col-10} or P_{dpy-7} and P_{col-19}:), none of

341   which resulted in significant axon breakage (Figure 4). Additionally, degradation of epidermal β-

342   spectrin did not affect the guidance or regrowth of axons after injury (Figure 4F). We did observe

343   a small fraction of L1:β-spectrinΔskin animals with small gaps in the dorsal nerve cord (Figure

344   4A,C,E). However, we hypothesize these gaps are due to instability of the axon tips, not breakage.

345   Gaps were not exacerbated by inhibition of regeneration (Figure 4C) as they are in L1:β-

346   spectrinΔneuron animals (Figure S3D). The DD and VD neurons each separately tile the dorsal

347   nerve cord, with the tips of adjoining processes connected by gap junctions. Epidermal β-spectrin

348   may function to promote or stabilize the establishment of this tiling pattern.

349   Recent results have suggested that β-spectrin in the epidermis is required to protect

350   against breakage in GABA neurons (Coakley et al., 2022). That study used the FLP-FRT system,

351   activated by the *dpy-7* epidermal promoter, to delete the *unc-70* gene in skin cells. However, in

352   addition to terminally-differentiated epidermal cells, *dpy-7* is also expressed earlier in the P cell

353   lineage, from which both epidermal cells and the VD GABA neurons are derived (Gilleard et al.,

15

354   1997; Sulston & Horvitz, 1977). Since FLP acts at the DNA level, when a precursor cell is edited,

355   all cells derived from it will also contain the edit. As a consequence, expression of FLP under the

356   *dpy-7* promoter would be expected to delete β-spectrin in both VD GABA neurons and in

357   epidermis. Thus, we hypothesize that in the previous experiments, as in ours, removal of β-

358   spectrin from GABA neurons results in axon breaks. Consistent with this result, previous work

359   showed rescue of β-spectrin in the epidermis did not rescue VD/DD neuron breakage in a loss-

360   of-function β-spectrin mutant (Hammarlund et al., 2007). Additional experiments will need to be

361   done to clarify the differences between these two methods of cell-specific targeted loss of β-

362   spectrin. Nevertheless, our results confirm the intrinsic importance of the MPS for VD/DD

363   GABAergic motor neuron integrity throughout lifespan.

364   **Loss of the GABAergic MPS as a model to study axon regeneration and degeneration *in***

365   ***vivo***

366   We show here that loss of β-spectrin from all neurons causes complete breakage of

367   VD/DD GABAergic neurons, and that loss of β-spectrin from only GABA neurons also results in

368   significant (though incomplete) breakage of VD/DD GABAergic neurons. In both cases, the

369   animals are much healthier than full body β-spectrin mutants (Hammarlund et al., 2000) which

370   have previously been used successfully in unbiased screens to identify conserved mediators of

371   axon regeneration (Hammarlund et al., 2009; Nix et al., 2014). Thus, these animals may enable

372   new approaches to studying axon regeneration and degeneration, in which targeted depletion of

373   neuronal β-spectrin is performed during development or in the mature nervous system to allow

374   for high throughput screening of genes or compounds that affect axon regeneration and

375   degeneration. In addition, the AID system may allow β-spectrin to be acutely degraded and then

376   the animals removed from auxin, preserving the stability of newly-synthesized β-spectrin and

377   allowing the study of MPS formation *in vivo*.

378   While previous studies have highlighted the importance of spectrin and the MPS for axon

379   regeneration (Hofmann et al., 2022), it is not possible to carefully discriminate if intrinsic β-

380   spectrin or the MPS promotes regeneration in our system because without β-spectrin axons

381   break; however, the robust growth cone formation in L1:β-spectrinΔneurons and L1:β-

382   spectrinΔGABA animals demonstrates intrinsic β-spectrin is not required for growth cone initiation

383   or outgrowth, consistent with previous data (Hammarlund et al., 2007, 2009; Nix et al., 2014). In

384   fact, it is possible that loss of β-spectrin may enhance axon regeneration. Disruption to the

385   cytoskeleton through destabilizing actin or microtubules has been shown to activate the DLK/JNK

386   pathway and mimic a pre-conditioning injury and promote axon regeneration (Valakh et al., 2015).

387   Thus, the robust regeneration we observe in neurons that lack β-spectrin may be due to

388   hyperactivation of DLK/JNK in L1:β-spectrinΔneurons animals.

389   Surprisingly, we observed that the MPS is disassembled hours before breakage and

390   degeneration occur. These data suggest that the MPS is not the only structure that promotes

391   neuronal integrity. We hypothesize that in the absence of the MPS, mechanical strain causes

392   damage to neurons to accumulate over time, eventually resulting in axonal breaks. Identifying

393   the processes downstream of MPS loss that control axon breakage would help elucidate how

394   axons act to preserve their integrity.

Methods

Caenorhabditis elegans

C. elegans were maintained on standard nematode growth media (NGM) seeded with *Escherichia coli* OP50 at 20°C unless otherwise stated. Hermaphrodites were used for all experiments. Males were used only for crosses. Strains used in this work are listed in Table S1.

Generation of transgenic animals

Transgenic animals were generated by microinjection (Stinchcomb et al., 1985). Promega 1kb DNA ladder was used as filler in the injection mix. In most cases, *P$_{myo-2}$::mCherry* (1.0 ng/uL) was used as a co-injection marker. Plasmids used to generate transgenics are listed in Table S2. Multicopy targeted insertion to generate the *wpIs495*[*P$_{rab-3}$::atTIR1::let-858UTR* + *P$_{myo-2}$::GFP*] allele was performed as previously described (El Mouridi et al., 2022). Briefly, we performed CRISPR-Cas9 mediated targeted extrachromosomal array integration into the modular safe-harbor transgene insertion landing site (moSCI) locus on chromosome IV in strain CFJ94. Successful integrates were screened for rescue of *unc-119* movement phenotype and insertion was verified by PCR (El Mouridi et al., 2022).

Molecular Cloning

Plasmids used for expression of transgenes in *C. elegans* were assembled into the destination vector pDEST™R4-R3 (Invitrogen) using Gateway recombination (Invitrogen). Entry clones for Gateway LR reactions were generated by Gibson Assembly (Gibson et al., 2009). All plasmids used in this work are listed in Table S2.

Auxin-inducible degradation

All auxin-induced knock-down experiments were performed by culturing animals on NGM plates containing 1 mM Auxin (#A10556.14; Thermo Fisher Scientific) seeded with OP50. Unless otherwise stated, gravid young adult animals were placed on 1mM Auxin plates and progeny were allowed to develop at 20°C. Animals of the same stage cultured on NGM plates lacking auxin

420   were controls. Because animals raised on 1mM Auxin to degrade pan-neuronal β-spectrin are

421   significantly smaller than control animals, visualization of vulva development was used to confirm

422   analysis was performed at the L4.4 – L4.7 stage unless otherwise stated (Mok et al., 2015). For

423   timed assays, one-day-old gravid adults were allowed to lay eggs on 1mM auxin-containing plates

424   or control plates for two hours. Adults were subsequently removed, and progeny were allowed to

425   develop at 20°C. Time 0 is defined as the start of the two-hour egg lay. Progeny were evaluated

426   at the late L1 stage, exactly 24 hours after the start of the egg lay. To degrade β-spectrin in the

427   mature nervous system, L4 stage animals were placed on 1mM Auxin plates (time 0) and

428   analyzed 24 hours (day 1 adult) or 48 hours (day 2 adult) later. L4 animals of the same genotype

429   placed on control NGM plates (time 0) served as controls.

430   **Fluorescence microscopy**

431   Animals were immobilized using 10mM Levamisole (Santa Cruz, sc-205730) and mounted on a

432   3% (wt/vol) agarose pad on a glass slide. Confocal imaging was performed using a laser Safe

433   DMi8 inverted microscope (Leica) equipped with a VT-iSIM system (BioVision), an ORCA-Flash

434   4.0 camera (Hamamatsu), HC PL APO 63x/1.40NA OIL CS2, a HC PL APO 40x/1.30NA OIL

435   CS2, a HC PL APO 20x/0.8NA AIR and HC PL APO 100x/ 1.47NA OIL objective as well as 488

436   nm, 561 nm and 637 nm laser lines. Image acquisition was controlled by MetaMorph Advanced

437   Confocal Acquisition Software Package. A step size of 0.2 μm was used. In cases where only

438   axon morphology or breakage was being assessed, we used an Olympus BX61 microscope with

439   attached Olympus DSU, Olympus UPlanFL N 40X/1.30 oil objective or UPlanSApo 60X/1.35 oil

440   objective, and Hamamatsu C11440 camera. Image acquisition was controlled by Micro-Manager

441   with a 0.4 μm step size.

442   **Analysis of fluorescence microscopy**

443   Raw images were processed and analyzed with Fiji/ImageJ v2.16.0/1.54g. Images were acquired

444   as a single image or multiple z layers and stacked into maximum projections using the maximum

445   intensity. To visualize the entire axon or animal that could not be captured in a single field of view,

446   multiple images were acquired and stitched together into a single image using the pairwise-

447   stitching plugin with a linear blending fusion method (Preibisch et al., 2009). Analysis was

448   performed on L4 stage animals unless otherwise noted.

449   **Quantification of axon breakage and gaps**

450   Axon breakage was identified as a discontinuity of the cytosolic fluorescent marker (GFP,

451   TagRFP, or chFP). Axons that were thin, dim, swollen, or beading were quantified as intact. If

452   these abnormal morphologies were present, they were quantified separately from breaks/gaps

453   and discussed as such in the results.

454   **Laser axotomy and quantification of axon regeneration**

455   Laser axotomy was performed as previously described (Byrne et al., 2011, 2014;

456   Kosmaczewski et al., 2015). Briefly, worms of the same genotype (strain XE3449) were allowed

457   to lay eggs on plates with 1mM auxin (L1:β-spectrinΔskin) and without (control). Progeny were

458   allowed to develop and larval stage L4.4-L4.6 animals carrying the wpEx570 array were mounted

459   on a 3% (wt/vol in M9 buffer) agarose pad, immobilized by 0.05 mm microbeads (Polysciences,

460   #08691) with 0.02% SDS, and visualized with a Nikon Eclipse 80i Microscope with a 100x Plan

461   Apo VC lens (1.4 NA). Fluorescently-labeled ventral type (VD) GABA motor neuron commissures

462   were severed at the dorsoventral midline using a 435 nm Photonic Instruments Micropoint laser

463   with 10 pulses at 20 Hz. Three to four of the seven most posterior commissures were severed per

464   worm. Worms were recovered at 20°C to NGM plates seeded with OP50 with 1mM auxin (L1:β-

465   spectrinΔskin) or without (control) and scored for axon regeneration 24 hours after axotomy.

466   To score regeneration, worms imaged by confocal microscopy. Images were blinded to

467   treatment group prior to analysis. Axon regeneration was scored as the relative length of regrowth.

468   This is defined as the vertical distance between the ventral nerve cord and the growth cone or

469   stump of the injured axon, normalized to the corresponding vertical distance between the dorsal

470   and ventral cords as previously described (Zeng et al., 2018). The relative lengths were measured

471   with ImageJ and plotted with GraphPad Prism. Full regeneration to the dorsal nerve cord

472   corresponds to a relative length value of 1. If an axon appeared to fuse with the distal stump, it

473   was given a score of full regeneration (relative length = 1). Because the data are not normally

474   distributed, the non-parametric Kolmogorov-Smirnov test was used to compare the cumulative

475   distribution of the normalized axon regrowth measurements between control and experimental

476   groups.

477   **Measurement of animal length and body morphology**

478   L4 animals were picked onto unseeded NGM plates and the plate was placed under a Leica

479   M165FC stereoscope. Still images of individual animals were captured with a Basler acA2440

480   camera controlled by the WormLab software. Images were analyzed in ImageJ and the length of

481   each worm was measured from the base of the tail to the mouth.

482   **Timed development assay**

483   Thirty Day 1 gravid adults were allowed to lay eggs for 2 hours on NGM plates with and without

484   1mM auxin. All adults were removed at the end of the 2 hours. Progeny were allowed to develop

485   at 20°C. The number of progeny reaching the L4 stage was quantified every two hours from 44

486   hours 64 hours, every two hours from 70 hours to 82 hours, and again at 94 hours and 98 hours.

487   Once a worm was counted as reaching the L4 stage it was removed from the plate to avoid double

488   counting. The average time of each animal to reach the L4 stage was quantified. The proportion

489   of animals reaching the L4 stage at each timepoint was graphed using GraphPad Prism and

490   compared using a log-rank (Mantel-Cox test). Any animal developmentally arrested and not

491   reaching the L4 stage by 98 hours was censored.

492   **Inhibition of DLK using a small molecular inhibitor**

493   DLK-1 was inhibited using the GNE-3511 inhibitor (MedChemExpress, HY-12947). The inhibitor

494   was dissolved in DMSO and added to 50°C NGM media at a final concentration of 50μM prior to

21

495   pouring. 1mM Auxin was also added to the media prior to pouring. Animals were allowed to lay

496   eggs on plates containing 1mM Auxin + 50μM GNE-3511. Progeny were allowed to develop and

497   were analyzed at the L4 stage.

Statistical analysis

499   All statistical analysis was performed in GraphPad Prism. For non-binary data, unless otherwise

500   noted, two-sided *t* test was used to compare two groups, and one-way ANOVA test followed by

501   Tukey's multiple comparisons test was used to compare multiple groups. Bar graphs depict

502   mean, and error bars show standard deviation. The number of animals scored for each

503   quantification is shown in or beside each dataset. Unless otherwise stated, data distributions

504   were assumed to be normal, but this was not formally tested. For relative length quantification of

505   regeneration following laser axotomy, data was not normally distributed; therefore, the non-

506   parametric Kolmogorov-Smirnov test was performed to compare cumulative distributions. For

507   binary data, Fisher's exact tests were performed.

Materials availability

509   Strains and plasmids used in this study are listed in Tables S1 and S2 respectively and will be

510   made available to the scientific community upon request directed to Dr. Hammarlund. Strains

511   generated in this study will be deposited at the Caenorhabditis Genetics Center (CGC).

Data availability

513   All data are available in the main text or the supplementary materials.

Acknowledgements

518

519

528

Author contributions

530   C.A. Davison, M. Hammarlund, and E.M. Jorgensen conceived the study. C.A. Davison performed

531   and analyzed all experiments in this study. D. Garcia helped generate many of the strains used

532   in this study and quantified axon breakage in multiple genotypes. C. Feng performed cloning,

533   confocal microscopy, and provided technical advice. H. Hao generated the XE3230 strain used

534   in this study and provided technical advice. The manuscript was written by C.A. Davison and M.

535   Hammarlund, with input from all coauthors.

Declarations of Interests

537   The authors declare no competing interests.

538

539

540

541   **References**

542   Ashley, G. E., Duong, T., Levenson, M. T., Martinez, M. A. Q., Johnson, L. C., Hibshman, J. D.,

543   Saeger, H. N., Palmisano, N. J., Doonan, R., Martinez-Mendez, R., Davidson, B. R.,

544   Zhang, W., Ragle, J. M., Medwig-Kinney, T. N., Sirota, S. S., Goldstein, B., Matus, D. Q.,

545   Dickinson, D. J., Reiner, D. J., & Ward, J. D. (2021). An expanded auxin-inducible

546   degron toolkit for Caenorhabditis elegans. *Genetics*, *217*(3), iyab006.

547   https://doi.org/10.1093/genetics/iyab006

548   Bonacossa-Pereira, I., Coakley, S., & Hilliard, M. A. (2022). Neuron-epidermal attachment

549   protects hyper-fragile axons from mechanical strain. *Cell Reports*, *38*(10), 110501.

550   https://doi.org/10.1016/j.celrep.2022.110501

551   Byrne, A. B., Edwards, T. J., & Hammarlund, M. (2011). In vivo Laser Axotomy in C. elegans.

552   *JoVE (Journal of Visualized Experiments)*, *51*, e2707. https://doi.org/10.3791/2707

553   Byrne, A. B., Walradt, T., Gardner, K. E., Hubbert, A., Reinke, V., & Hammarlund, M. (2014).

554   Insulin/IGF1 Signaling Inhibits Age-Dependent Axon Regeneration. *Neuron*, *81*(3), 561–

555   573. https://doi.org/10.1016/j.neuron.2013.11.019

556   Català-Castro, F., Bonilla-Quintana, M., Sanfeliu-Cerdán, N., Rangamani, P., & Krieg, M.

557   (2025). *Periodic Obstacles Regulate Membrane Tension Propagation to Enable*

558   *Localized Mechanotransduction* (p. 2025.01.14.632796). bioRxiv.

559   https://doi.org/10.1101/2025.01.14.632796

560   Chalfie, M., & Sulston, J. (1981). Developmental genetics of the mechanosensory neurons of

561   *Caenorhabditis elegans. Developmental Biology*, *82*(2), 358–370.

562   https://doi.org/10.1016/0012-1606(81)90459-0

563   Chisholm, A. D., & Xu, S. (2012). The Caenorhabditis elegans epidermis as a model skin. II:

564   Differentiation and physiological roles. *WIREs Developmental Biology*, *1*(6), 879–902.

565   https://doi.org/10.1002/wdev.77

566 Coakley, S., Bonacossa-Pereira, I., & Hilliard, M. A. (2022). *Spectrin forms a periodic*

567   *cytoskeleton within the epidermis to preserve axonal integrity* (p. 2022.09.07.507048).

568   bioRxiv. https://doi.org/10.1101/2022.09.07.507048

569 Coakley, S., Ritchie, F. K., Galbraith, K. M., & Hilliard, M. A. (2020). Epidermal control of axonal

570   attachment via β-spectrin and the GTPase-activating protein TBC-10 prevents axonal

571   degeneration. *Nature Communications*, *11*(1), 133. https://doi.org/10.1038/s41467-019-

572   13795-x

573 Costa, A. R., Sousa, S. C., Pinto-Costa, R., Mateus, J. C., Lopes, C. D., Costa, A. C., Rosa, D.,

574   Machado, D., Pajuelo, L., Wang, X., Zhou, F., Pereira, A. J., Sampaio, P., Rubinstein, B.

575   Y., Mendes Pinto, I., Lampe, M., Aguiar, P., & Sousa, M. M. (2020). The membrane

576   periodic skeleton is an actomyosin network that regulates axonal diameter and

577   conduction. *eLife*, *9*, e55471. https://doi.org/10.7554/eLife.55471

578 Das, R., Lin, L.-C., Català-Castro, F., Malaiwong, N., Sanfeliu-Cerdán, N., Porta-de-la-Riva, M.,

579   Pidde, A., & Krieg, M. (2021). An asymmetric mechanical code ciphers curvature-

580   dependent proprioceptor activity. *Science Advances*, *7*(38), eabg4617.

581   https://doi.org/10.1126/sciadv.abg4617

582 D'Este, E., Kamin, D., Göttfert, F., El-Hady, A., & Hell, S. W. (2015). STED Nanoscopy Reveals

583   the Ubiquity of Subcortical Cytoskeleton Periodicity in Living Neurons. *Cell Reports*,

584   *10*(8), 1246–1251. https://doi.org/10.1016/j.celrep.2015.02.007

585 Dubey, S., Bhembre, N., Bodas, S., Veer, S., Ghose, A., Callan-Jones, A., & Pullarkat, P.

586   (2020). The axonal actin-spectrin lattice acts as a tension buffering shock absorber.

587   *eLife*, *9*, e51772. https://doi.org/10.7554/eLife.51772

588 Edwards, T. J., & Hammarlund, M. (2014). Syndecan Promotes Axon Regeneration by

589   Stabilizing Growth Cone Migration. *Cell Reports*, *8*(1), 272–283.

590   https://doi.org/10.1016/j.celrep.2014.06.008

591 El Mouridi, S., Alkhaldi, F., & Frøkjær-Jensen, C. (2022). Modular safe-harbor transgene

592   insertion for targeted single-copy and extrachromosomal array integration in

593   Caenorhabditis elegans. *G3 Genes|Genomes|Genetics*, *12*(9), jkac184.

594   https://doi.org/10.1093/g3journal/jkac184

595 Garcia-Fresco, G. P., Sousa, A. D., Pillai, A. M., Moy, S. S., Crawley, J. N., Tessarollo, L.,

596   Dupree, J. L., & Bhat, M. A. (2006). Disruption of axo–glial junctions causes cytoskeletal

597   disorganization and degeneration of Purkinje neuron axons. *Proceedings of the National*

598   *Academy of Sciences*, *103*(13), 5137–5142. https://doi.org/10.1073/pnas.0601082103

599 Gibson, D. G., Young, L., Chuang, R.-Y., Venter, J. C., Hutchison, C. A., & Smith, H. O. (2009).

600   Enzymatic assembly of DNA molecules up to several hundred kilobases. *Nature*

601   *Methods*, *6*(5), 343–345. https://doi.org/10.1038/nmeth.1318

602 Gilleard, J. S., Barry, J. D., & Johnstone, I. L. (1997). Cis Regulatory Requirements for

603   Hypodermal Cell-Specific Expression of the Caenorhabditis elegans Cuticle Collagen

604   Gene dpy-7. *Molecular and Cellular Biology*, *17*(4), 2301–2311.

605   https://doi.org/10.1128/MCB.17.4.2301

606 Glomb, O., Swaim, G., LLancao, P. M., Lovejoy, C., Sutradhar, S., Park, J., Wu, Y., Cason, S.

607   E., Holzbaur, E. L. F., Hammarlund, M., Howard, J., Ferguson, S. M., Gramlich, M. W., &

608   Yogev, S. (2023). A kinesin-1 adaptor complex controls bimodal slow axonal transport of

609   spectrin in Caenorhabditis elegans. *Developmental Cell*, *58*(19), 1847-1863.e12.

610   https://doi.org/10.1016/j.devcel.2023.08.031

611 Hallam, S. J., & Jin, Y. (1998). Lin-14 regulates the timing of synaptic remodelling in

612   Caenorhabditis elegans. *Nature*, *395*(6697), 78–82. https://doi.org/10.1038/25757

613 Hammarlund, M., Davis, W. S., & Jorgensen, E. M. (2000). Mutations in β-Spectrin Disrupt Axon

614   Outgrowth and Sarcomere Structure. *Journal of Cell Biology*, *149*(4), 931–942.

615   https://doi.org/10.1083/jcb.149.4.931

616   Hammarlund, M., Jorgensen, E. M., & Bastiani, M. J. (2007). Axons break in animals lacking β-

617   spectrin. *Journal of Cell Biology*, *176*(3), 269–275. https://doi.org/10.1083/jcb.200611117

618   Hammarlund, M., Nix, P., Hauth, L., Jorgensen, E. M., & Bastiani, M. (2009). Axon

619   Regeneration Requires a Conserved MAP Kinase Pathway. *Science*, *323*(5915), 802–

620   806. https://doi.org/10.1126/science.1165527

621   He, J., Zhou, R., Wu, Z., Carrasco, M. A., Kurshan, P. T., Farley, J. E., Simon, D. J., Wang, G.,

622   Han, B., Hao, J., Heller, E., Freeman, M. R., Shen, K., Maniatis, T., Tessier-Lavigne, M.,

623   & Zhuang, X. (2016). Prevalent presence of periodic actin–spectrin-based membrane

624   skeleton in a broad range of neuronal cell types and animal species. *Proceedings of the*

625   *National Academy of Sciences*, *113*(21), 6029–6034.

626   https://doi.org/10.1073/pnas.1605707113

627   Hofmann, M., Biller, L., Michel, U., Bähr, M., & Koch, J. C. (2022). Cytoskeletal assembly in

628   axonal outgrowth and regeneration analyzed on the nanoscale. *Scientific Reports*, *12*(1),

629   14387. https://doi.org/10.1038/s41598-022-18562-5

630   Holland, A. J., Fachinetti, D., Han, J. S., & Cleveland, D. W. (2012). Inducible, reversible system

631   for the rapid and complete degradation of proteins in mammalian cells. *Proceedings of*

632   *the National Academy of Sciences*, *109*(49), E3350–E3357.

633   https://doi.org/10.1073/pnas.1216880109

634   Huang, C. Y.-M., Zhang, C., Ho, T. S.-Y., Oses-Prieto, J., Burlingame, A. L., Lalonde, J.,

635   Noebels, J. L., Leterrier, C., & Rasband, M. N. (2017). αII Spectrin Forms a Periodic

636   Cytoskeleton at the Axon Initial Segment and Is Required for Nervous System Function.

637   *Journal of Neuroscience*, *37*(47), 11311–11322.

638   https://doi.org/10.1523/JNEUROSCI.2112-17.2017

639   Huang, C. Y.-M., Zhang, C., Zollinger, D. R., Leterrier, C., & Rasband, M. N. (2017). An αII

640   Spectrin-Based Cytoskeleton Protects Large-Diameter Myelinated Axons from

641   Degeneration. *Journal of Neuroscience*, *37*(47), 11323–11334.

642   https://doi.org/10.1523/JNEUROSCI.2113-17.2017

643 Hülsmeier, J., Pielage, J., Rickert, C., Technau, G. M., Klämbt, C., & Stork, T. (2007). Distinct

644   functions of α-Spectrin and β-Spectrin during axonal pathfinding. *Development*, *134*(4),

645   713–722. https://doi.org/10.1242/dev.02758

646 Ikeda, Y., Dick, K. A., Weatherspoon, M. R., Gincel, D., Armbrust, K. R., Dalton, J. C., Stevanin,

647   G., Dürr, A., Zühlke, C., Bürk, K., Clark, H. B., Brice, A., Rothstein, J. D., Schut, L. J.,

648   Day, J. W., & Ranum, L. P. W. (2006). Spectrin mutations cause spinocerebellar ataxia

649   type 5. *Nature Genetics*, *38*(2), 184–190. https://doi.org/10.1038/ng1728

650 Jia, R., Li, D., Li, M., Chai, Y., Liu, Y., Xie, Z., Shao, W., Xie, C., Li, L., Huang, X., Chen, L., Li,

651   W., & Ou, G. (2019). Spectrin-based membrane skeleton supports ciliogenesis. *PLOS*

652   *Biology*, *17*(7), e3000369. https://doi.org/10.1371/journal.pbio.3000369

653 Kalichamy, S. S., Alcantara, A. V., Kim, B.-S., Park, J., Yoon, K., & Lee, J. I. (2020). Muscle and

654   epidermal contributions of the structural protein β-spectrin promote hypergravity-induced

655   motor neuron axon defects in C. elegans. *Scientific Reports*, *10*(1), 21214.

656   https://doi.org/10.1038/s41598-020-78414-y

657 Knobel, K. M., Jorgensen, E. M., & Bastiani, M. J. (1999). Growth cones stall and collapse

658   during axon outgrowth in Caenorhabditis elegans. *Development*, *126*(20), 4489–4498.

659   https://doi.org/10.1242/dev.126.20.4489

660 Kosmaczewski, S. G., Han, S. M., Han, B., Irving Meyer, B., Baig, H. S., Athar, W., Lin-Moore,

661   A. T., Koelle, M. R., & Hammarlund, M. (2015). RNA ligation in neurons by RtcB inhibits

662   axon regeneration. *Proceedings of the National Academy of Sciences*, *112*(27), 8451–

663   8456. https://doi.org/10.1073/pnas.1502948112

664 Krieg, M., Dunn, A. R., & Goodman, M. B. (2014). Mechanical control of the sense of touch by

665   β-spectrin. *Nature Cell Biology*, *16*(3), 224–233. https://doi.org/10.1038/ncb2915

666   Krieg, M., Stühmer, J., Cueva, J. G., Fetter, R., Spilker, K., Cremers, D., Shen, K., Dunn, A. R.,

667   & Goodman, M. B. (2017). Genetic defects in β-spectrin and tau sensitize C. elegans

668   axons to movement-induced damage via torque-tension coupling. *eLife*, *6*, e20172.

669   https://doi.org/10.7554/eLife.20172

670   Liu, C.-H., Stevens, S. R., Teliska, L. H., Stankewich, M., Mohler, P. J., Hund, T. J., & Rasband,

671   M. N. (2020). Nodal β spectrins are required to maintain Na+ channel clustering and

672   axon integrity. *eLife*, *9*, e52378. https://doi.org/10.7554/eLife.52378

673   Lorenzo, D. N., Badea, A., Zhou, R., Mohler, P. J., Zhuang, X., & Bennett, V. (2019). βII-spectrin

674   promotes mouse brain connectivity through stabilizing axonal plasma membranes and

675   enabling axonal organelle transport. *Proceedings of the National Academy of Sciences*,

676   *116*(31), 15686–15695. https://doi.org/10.1073/pnas.1820649116

677   Lorenzo, D. N., Edwards, R. J., & Slavutsky, A. L. (2023). Spectrins: Molecular organizers and

678   targets of neurological disorders. *Nature Reviews Neuroscience*, *24*(4), 195–212.

679   https://doi.org/10.1038/s41583-022-00674-6

680   Lorenzo, D. N., Li, M., Mische, S. E., Armbrust, K. R., Ranum, L. P. W., & Hays, T. S. (2010).

681   Spectrin mutations that cause spinocerebellar ataxia type 5 impair axonal transport and

682   induce neurodegeneration in Drosophila. *Journal of Cell Biology*, *189*(1), 143–158.

683   https://doi.org/10.1083/jcb.200905158

684   Mok, D. Z. L., Sternberg, P. W., & Inoue, T. (2015). Morphologically defined sub-stages of C.

685   elegans vulval development in the fourth larval stage. *BMC Developmental Biology*, *15*,

686   26. https://doi.org/10.1186/s12861-015-0076-7

687   Negishi, T., Asakawa, M., Kanemaki, M. T., & Sawa, H. (2019). Modified auxin improves the

688   auxin-inducible degradation (AID) system for laid C. elegans embryos. *microPublication*

689   *Biology*. https://doi.org/10.17912/micropub.biology.000190

690   Nix, P., Hammarlund, M., Hauth, L., Lachnit, M., Jorgensen, E. M., & Bastiani, M. (2014). Axon

691   Regeneration Genes Identified by RNAi Screening in C. elegans. *Journal of*

692   *Neuroscience*, *34*(2), 629–645. https://doi.org/10.1523/JNEUROSCI.3859-13.2014

693   Preibisch, S., Saalfeld, S., & Tomancak, P. (2009). Globally optimal stitching of tiled 3D

694   microscopic image acquisitions. *Bioinformatics*, *25*(11), 1463–1465.

695   https://doi.org/10.1093/bioinformatics/btp184

696   Speicher, D. W., & Marchesi, V. T. (1984). Erythrocyte spectrin is comprised of many

697   homologous triple helical segments. *Nature*, *311*(5982), 177–180.

698   https://doi.org/10.1038/311177a0

699   Sternberg, P. W., Van Auken, K., Wang, Q., Wright, A., Yook, K., Zarowiecki, M., Arnaboldi, V.,

700   Becerra, A., Brown, S., Cain, S., Chan, J., Chen, W. J., Cho, J., Davis, P., Diamantakis,

701   S., Dyer, S., Grigoriadis, D., Grove, C. A., Harris, T., … Stein, L. (2024). WormBase

702   2024: Status and transitioning to Alliance infrastructure. *Genetics*, *227*(1), iyae050.

703   https://doi.org/10.1093/genetics/iyae050

704   Stinchcomb, D. T., Shaw, J. E., Carr, S. H., & Hirsh, D. (1985). Extrachromosomal DNA

705   Transformation of Caenorhabditis elegans. *Molecular and Cellular Biology*, *5*(12), 3484–

706   3496. https://doi.org/10.1128/mcb.5.12.3484-3496.1985

707   Sulston, J. E., & Brenner, S. (1997). Post-embryonic development in the ventral cord of

708   Caenorhabditis elegans. *Philosophical Transactions of the Royal Society of London. B,*

709   *Biological Sciences*, *275*(938), 287–297. https://doi.org/10.1098/rstb.1976.0084

710   Sulston, J. E., & Horvitz, H. R. (1977). Post-embryonic cell lineages of the nematode,

711   *Caenorhabditis elegans*. *Developmental Biology*, *56*(1), 110–156.

712   https://doi.org/10.1016/0012-1606(77)90158-0

713   Susuki, K., Raphael, A. R., Ogawa, Y., Stankewich, M. C., Peles, E., Talbot, W. S., & Rasband,

714   M. N. (2011). Schwann cell spectrins modulate peripheral nerve myelination.

715   *Proceedings of the National Academy of Sciences*, *108*(19), 8009–8014.

716   https://doi.org/10.1073/pnas.1019600108

717   Susuki, K., Zollinger, D. R., Chang, K.-J., Zhang, C., Huang, C. Y.-M., Tsai, C.-R., Galiano, M.

718   R., Liu, Y., Benusa, S. D., Yermakov, L. M., Griggs, R. B., Dupree, J. L., & Rasband, M.

719   N. (2018). Glial βII Spectrin Contributes to Paranode Formation and Maintenance.

720   *Journal of Neuroscience*, *38*(27), 6063–6075. https://doi.org/10.1523/JNEUROSCI.3647-

721   17.2018

722   Taylor, S. R., Santpere, G., Weinreb, A., Barrett, A., Reilly, M. B., Xu, C., Varol, E., Oikonomou,

723   P., Glenwinkel, L., McWhirter, R., Poff, A., Basavaraju, M., Rafi, I., Yemini, E., Cook, S.

724   J., Abrams, A., Vidal, B., Cros, C., Tavazoie, S., … Miller, D. M. (2021). Molecular

725   topography of an entire nervous system. *Cell*, *184*(16), 4329-4347.e23.

726   https://doi.org/10.1016/j.cell.2021.06.023

727   Valakh, V., Frey, E., Babetto, E., Walker, L. J., & DiAntonio, A. (2015). Cytoskeletal disruption

728   activates the DLK/JNK pathway, which promotes axonal regeneration and mimics a

729   preconditioning injury. *Neurobiology of Disease*, *77*, 13–25.

730   https://doi.org/10.1016/j.nbd.2015.02.014

731   Wang, C., Yang, Y., Fu, R., Zhu, Y., & Zhang, H. (2020). Periodic subcellular structures undergo

732   long-range synchronized reorganization during C. elegans epidermal development.

733   *Journal of Cell Science*, *133*(21), jcs246793. https://doi.org/10.1242/jcs.246793

734   Wernert, F., Moparthi, S. B., Pelletier, F., Lainé, J., Simons, E., Moulay, G., Rueda, F., Jullien,

735   N., Benkhelifa-Ziyyat, S., Papandréou, M.-J., Leterrier, C., & Vassilopoulos, S. (2024).

736   The actin-spectrin submembrane scaffold restricts endocytosis along proximal axons.

737   *Science*, *385*(6711), eado2032. https://doi.org/10.1126/science.ado2032

738   White, J. G., Albertson, D. G., & Anness, M. a. R. (1978). Connectivity changes in a class of

739   motoneurone during the development of a nematode. *Nature*, *271*(5647), 764–766.

740   https://doi.org/10.1038/271764a0

741   White, J. G., Southgate, E., Thomson, J. N., & Brenner, S. (1997). The structure of the ventral

742   nerve cord of Caenorhabditis elegans. *Philosophical Transactions of the Royal Society*

743   *of London. B, Biological Sciences*, *275*(938), 327–348.

744   https://doi.org/10.1098/rstb.1976.0086

745   Xu, K., Zhong, G., & Zhuang, X. (2013). Actin, Spectrin, and Associated Proteins Form a

746   Periodic Cytoskeletal Structure in Axons. *Science*, *339*(6118), 452–456.

747   https://doi.org/10.1126/science.1232251

748   Yan, Y., Winograd, E., Viel, A., Cronin, T., Harrison, S. C., & Branton, D. (1993). Crystal

749   Structure of the Repetitive Segments of Spectrin. *Science*, *262*(5142), 2027–2030.

750   https://doi.org/10.1126/science.8266097

751   Zeng, L., Bejjani, R. E., & Hammarlund, M. (2018). *The Amyloid Precursor-like Protein APL-1*

752   *Regulates Axon Regeneration* (p. 305284). bioRxiv. https://doi.org/10.1101/305284

753   Zhang, C., Susuki, K., Zollinger, D. R., Dupree, J. L., & Rasband, M. N. (2013). Membrane

754   domain organization of myelinated axons requires βII spectrin. *Journal of Cell Biology*,

755   *203*(3), 437–443. https://doi.org/10.1083/jcb.201308116

756   Zhang, L., Ward, J. D., Cheng, Z., & Dernburg, A. F. (2015). The auxin-inducible degradation

757   (AID) system enables versatile conditional protein depletion in *C. elegans*. *Development*,

758   dev.129635. https://doi.org/10.1242/dev.129635

759

760
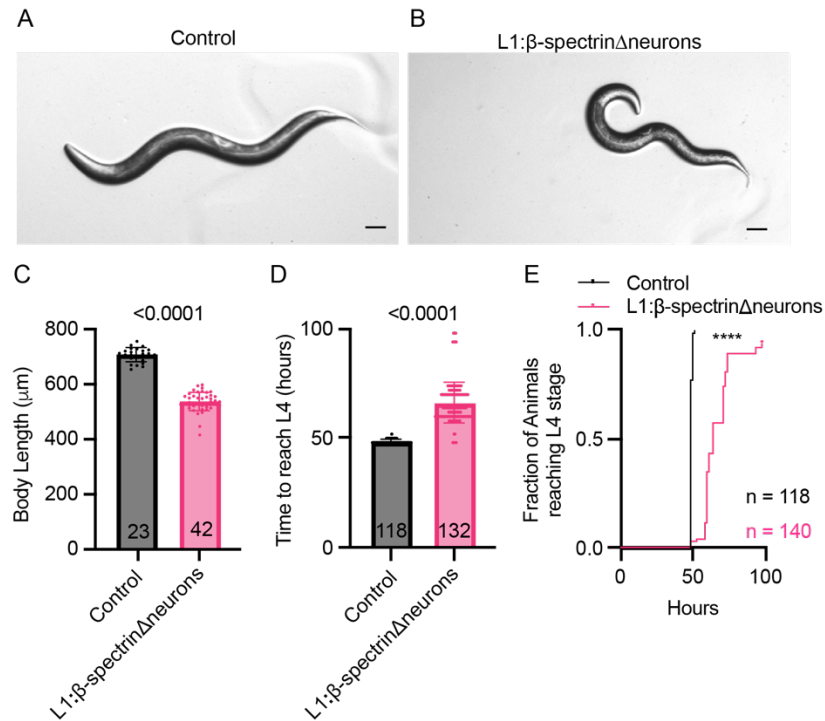
Figure 1: Degradation of neuronal β-spectrin from early larval stage causes morphological and developmental phenotypes

Representative images of L4 stage control animals homozygous for *unc-70::AID* and $P_{rab-3}::atTIR1$ and raised on (A) control or (B) 1mM auxin (IAA) to degrade β-spectrin from all neurons from the L1 stage (L1:β-spectrinΔneurons). Strain XE3230. Scale bar 50μm.

(C) Quantification of the body length of control (mean = 704 μm) and L1:β-spectrinΔneurons animals (mean = 534 μm) at the L4 stage. (unpaired two-tailed t-test: p<0.0001).

(D) Quantification of the number of hours from egg lay to the L4 stage at 20°C in control (mean = 48.49 hours) and L1:β-spectrinΔneurons (mean = 65.95 hours) (unpaired two-tailed t-test: p<0.0001). Eight additional (5.7% of total) L1:β-spectrinΔneurons animals arrested at the L1/L2 stage and were censored at 98 hours.

(E) Hours from egg lay to reach the L4 stage represented as a cumulative fraction of animals (Log-rank Mantel-Cox test: p<0.0001)

33

774   The number of animals scored for each quantification is shown in or beside each dataset. Error

775   bars show the standard deviation.

776
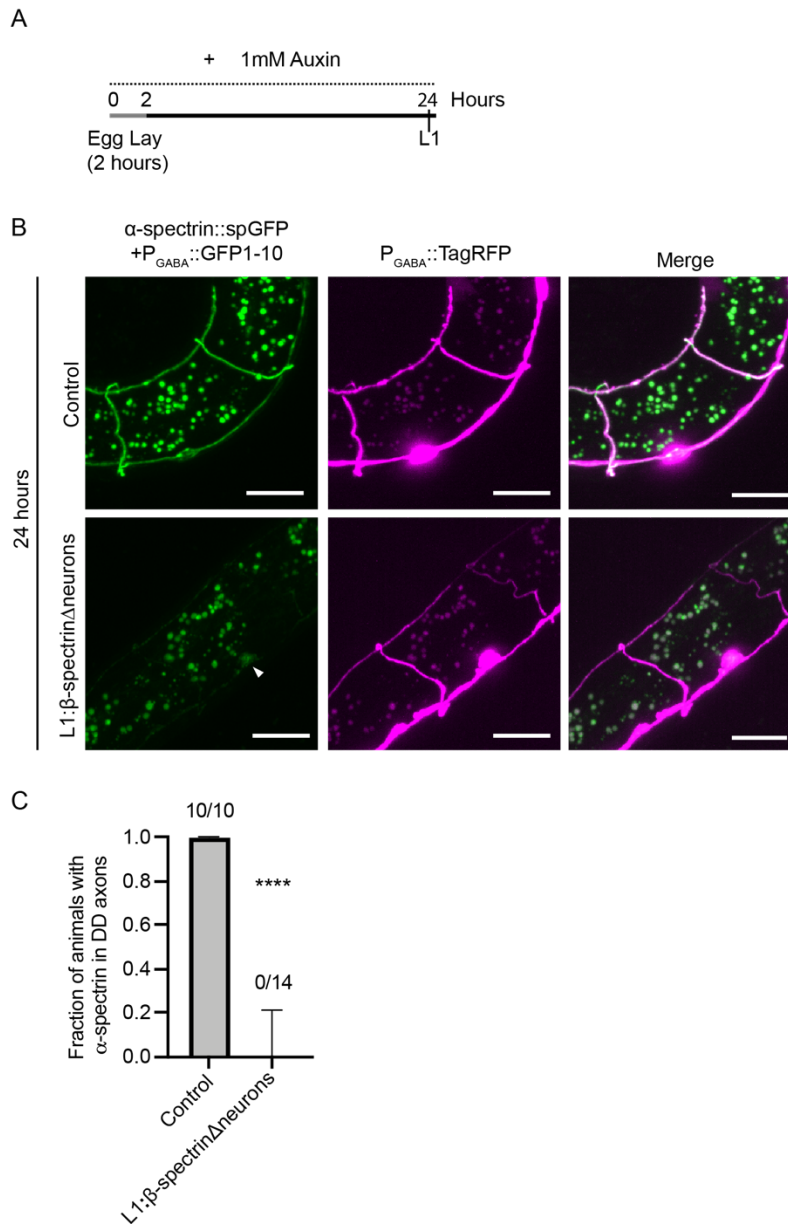
Figure 2: Degradation of neuronal β-spectrin disrupts the MPS within 24 hours

(A) Schematic of degradation timing for L1:β-spectrinΔneurons assayed at the L1 stage

(B) Representative images of endogenous α-spectrin in GABA neurons (split-GFP labeled) and

GABA neuron morphology (cytosolic TagRFP) in L1 control (no auxin) and L1:β-

spectrinΔneurons animals (1mM auxin for 24 hours). Scale bar 10 μm. The white arrow points

towards accumulated α-spectrin in cell body of L1:β-spectrinΔneurons animal.

784   (C) Quantification of the fraction of animals with endogenous α–spectrin visible in any DD

785   neuron commissure at the 24-hour time point (Fisher's exact test: p<0.0001). The number of

786   animals scored is shown above each bar.

787
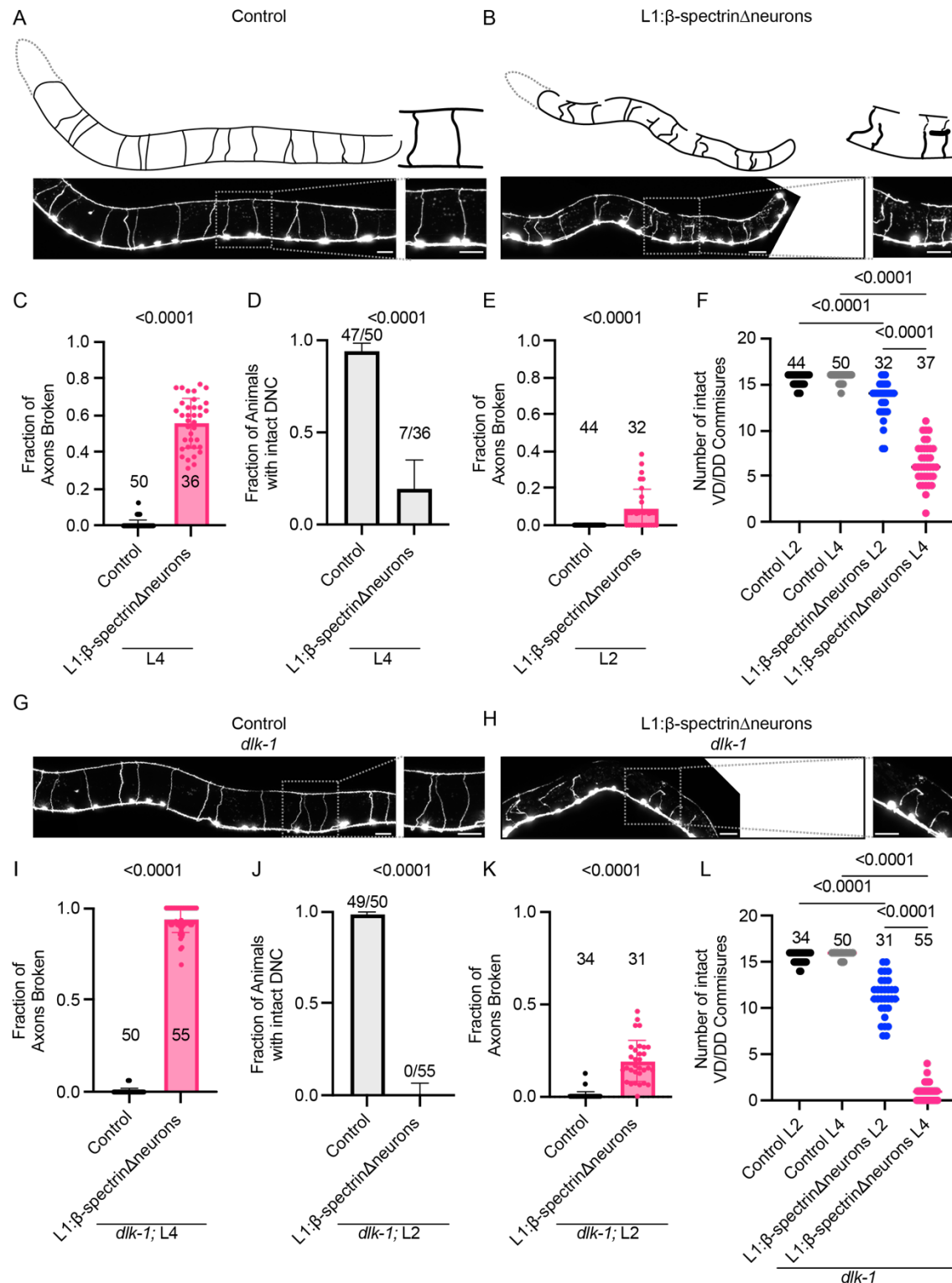
Figure 3: VD/DD axons break when neurons lack β-spectrin

789   (A-B) Representative images and cartoon tracings of VD/DD GABA neurons in (A) L4 stage

790   control (no auxin) and (B) L4 animal raised on 1mM Auxin to degrade β-spectrin from all

791   neurons from the L1 stage (L1:β-spectrinΔneurons). Strain XE3230. Scale bar 20μm.

792   (C) Quantification of the fraction of axons broken per animal in L4 stage control and L1:β-

793   spectrinΔneurons animals (unpaired two-tailed t-test: p<0.0001).

794   (D) Quantification of the fraction of animals with an intact dorsal nerve cord (DNC) in L4 stage

795   control and L1:β-spectrinΔneurons animals (Fisher's exact test: p<0.0001).

796   (E) Quantification of the fraction of axons broken per animal in L2 stage control and L1:β-

797   spectrinΔneurons (unpaired two-tailed t-test: p<0.0001)

798   (F) Quantification of the number of visible intact VD/DD commissures observed in L2 and L4

799   stage control and L1:β-spectrinΔneurons animals (One-way ANOVA followed by Tukey's

800   multiple comparisons test p<0.0001).

801   (G-H) Representative image of VD/DD GABA neurons in L4 stage (G) *dlk-1* loss of function

802   control (no auxin) and (H) *dlk-1* animal raised on 1mM Auxin to degraded β-spectrin from all

803   neurons from the L1 stage (L1:β-spectrinΔneurons), Strain XE3303. Scale bar 20μm.

804   (I) Quantification of the fraction of axons broken per animal in L4 stage *dlk-1* control and *dlk-1;*

805   L1:β-spectrinΔneurons animals (unpaired two-tailed t-test: p<0.0001).

806   (J) Quantification of the fraction of animals with an intact DNC in L4 stage *dlk-1* control and *dlk-*

807   *1;* L1:β-spectrinΔneurons animals (Fisher's exact test: p<0.0001)

808   (K) Quantification of the fraction of axons broken per animal in L2 stage *dlk-1* control and *dlk-1;*

809   L1:β-spectrinΔneurons animals (unpaired two-tailed t-test: p<0.0001).

810   (L) Quantification of the number of intact VD/DD commissures observed in L2 and L4 control

811   *dlk-1* and *dlk-1;* L1:β-spectrinΔneurons animals (ANOVA followed by Tukey's multiple

812   comparisons test: p<0.0001).

813   The number of animals scored for each quantification is shown in or above each bar.
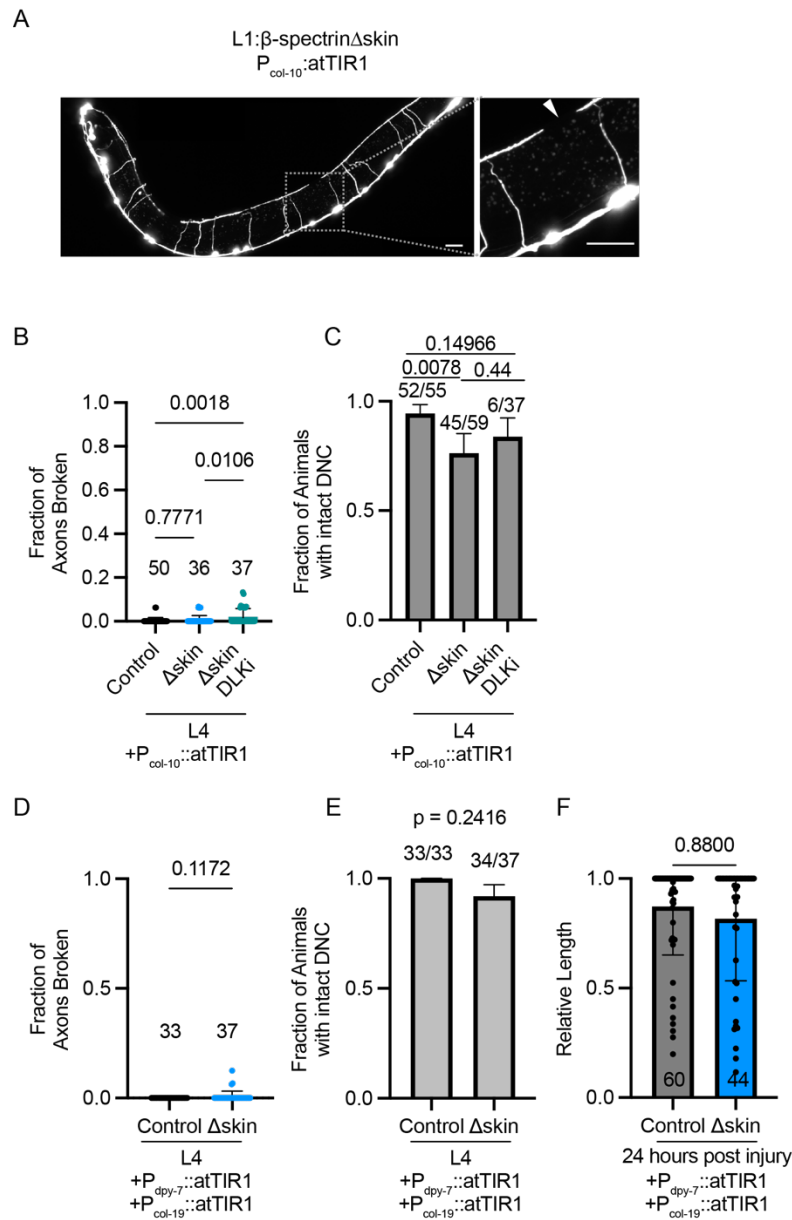
Figure 4: Epidermal β-spectrin is not required for GABA neuron integrity or regeneration

(A) Representative image of GABA neurons in L4 animal when β-spectrin is degraded from the epidermis ($P_{col-10}::atTIR1$ + 1mM Auxin) from the L1 stage (L1:β-spectrinΔskin). Scale bar 20μm. White arrow indicates gap in dorsal nerve cord.

819 (B) Quantification of the fraction of axons broken when β-spectrin is degraded from the

820 epidermis (L1:β-spectrinΔskin) using $P_{col-10}::atTIR1$ with and without inhibition of DLK (DLKi –

821 50μM GNE-3511). (ANOVA followed by Tukey's multiple comparisons test).

822 (C) Quantification of the fraction of animals with an intact dorsal nerve cord (DNC) in control,

823 L1:β-spectrinΔskin, and L1:β-spectrinΔskin + DLKi using $P_{col-10}::atTIR1$ (Fisher's Exact tests)

824 (D) Quantification of the fraction of axons broken when β-spectrin is degraded from the

825 epidermis (L1:β-spectrinΔskin) using $P_{dpy-7}::atTIR1$ and $P_{col-19}::atTIR1$ (unpaired two-tailed t-test:

826 non-significant p = 0.1172).

827 (E) Quantification of the fraction of animals with an intact dorsal nerve cord (DNC) in control and

828 L1:β-spectrinΔskin using $P_{dpy-7}::atTIR1$ and $P_{col-19}::atTIR1$ (Fisher's Exact test: p = 0.2416)

829 (F) Quantification of axon regeneration as the relative length of regrowth 24 hours after laser-

830 axotomy induced injury in control and Δskin animals (Kolmogorov-Smirnov test: nonsignificant

831 p=0.88).
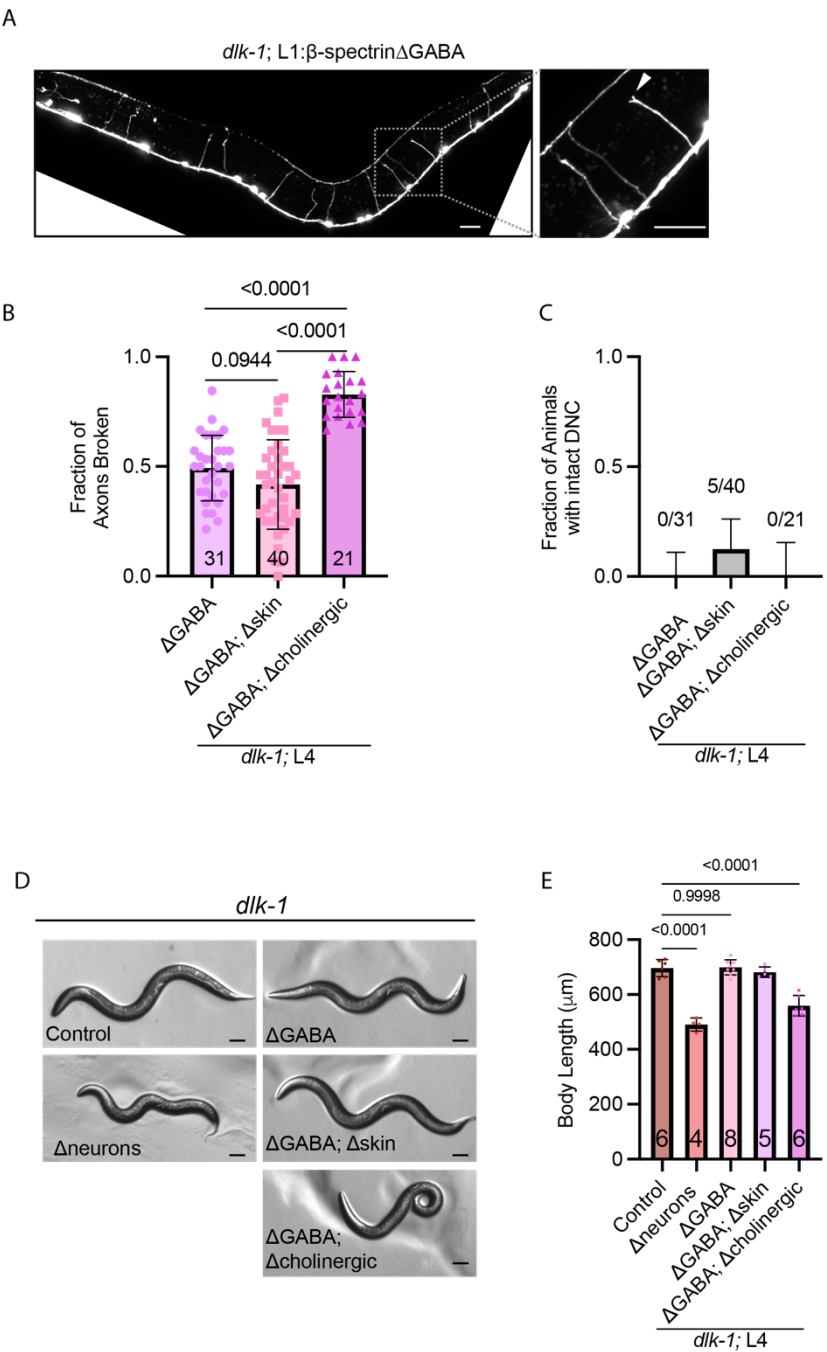
Figure 5: β-spectrin in cholinergic neurons modulates the effect of GABA neuron spectrin loss on axon integrity

835   (A) Representative image of *dlk-1* animal raised on 1mM Auxin to degraded β-spectrin from

836   GABA neurons only (L1:β-spectrinΔGABA). Scale bar 20μm. White arrow indicates broken

837   axon.

838   (B) Quantification of the fraction of axons broken per animal in L4 *dlk-1* animals when β-spectrin

839   is degraded from GABA neurons only ($P_{unc-47}::atTIR1$), GABA neurons and the skin (P_{unc-}

840     $_{47}::atTIR1$, $P_{dpy-7}::atTIR1$ and $P_{col-19}::atTIR$), and GABA neurons and cholinergic neurons (P_{unc-}

841     $_{47}::atTIR1$, $P_{unc-17}::atTIR1$) (ANOVA followed Tukey's multiple comparisons test: $p < 0.0001$)

842   (C) Quantification of the fraction of animals with an intact dorsal nerve cord (DNC) when β-

843   spectrin is degraded from GABA neurons only, GABA neurons and the skin, and GABA neurons

844   and cholinergic neurons

845   (D) Representative images of body morphology and (E) quantification of body length in L4 stage

846   animals when β-spectrin is degraded from all neurons, GABA neurons, GABA neurons and skin,

847   and GABA neurons and cholinergic neurons in the *dlk-1* loss of function background. Scale bar

848   50μm. Control animals contain the $P_{rab-3}::atTIR1$ allele but were not exposed to auxin. (ANOVA

849   followed Tukey's multiple comparisons test: $p < 0.0001$).
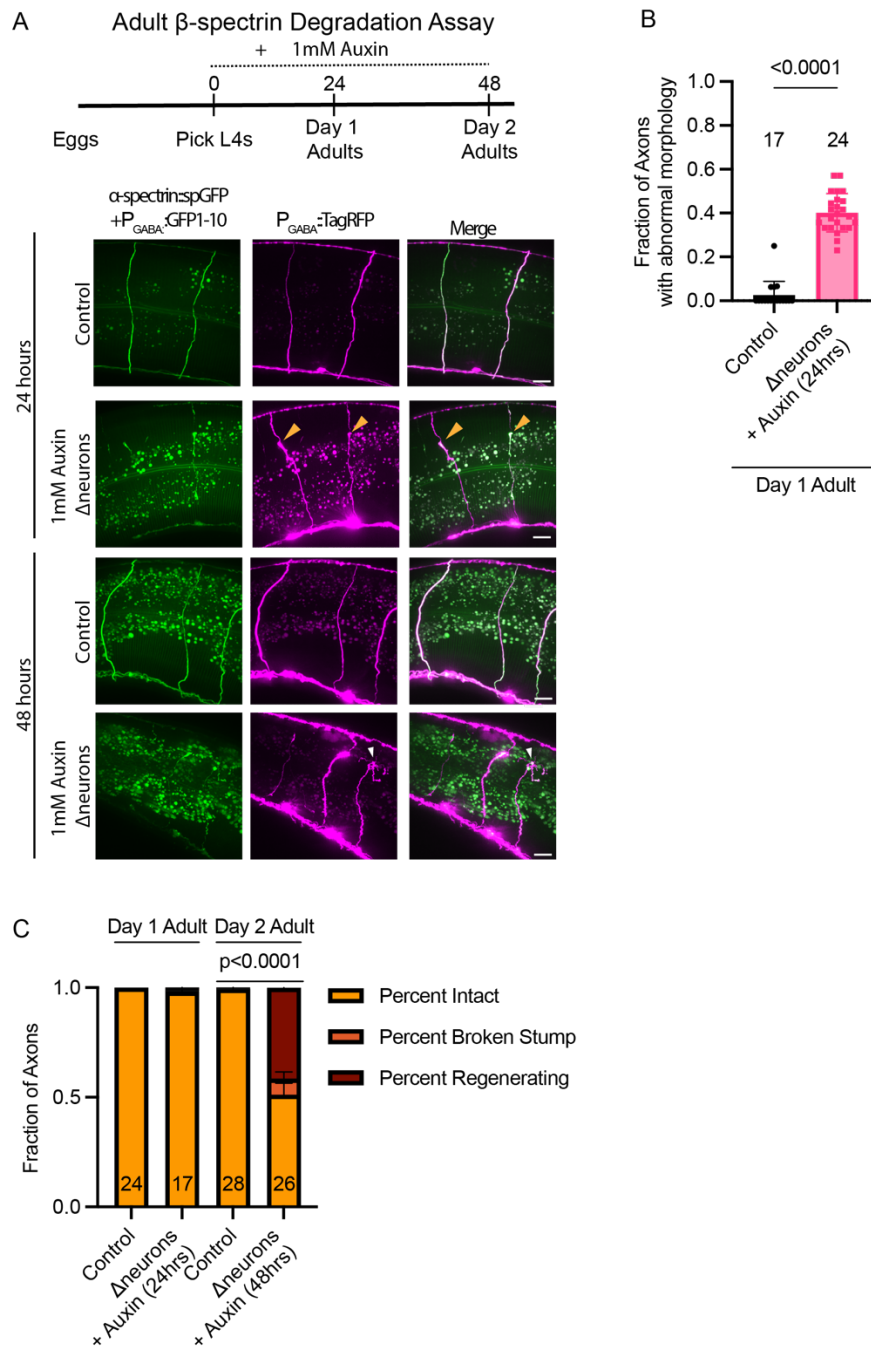
Figure 6: Spectrin is required in mature neurons to prevent axon breaks

(A) Adult β-spectrin degradation assay: Representative images of endogenous α-spectrin in

GABA neurons (split-GFP) and GABA neuron morphology (cytosolic TagRFP) in day 1 and day

2 control and β-spectrinΔneurons adults when β-spectrin is degraded starting at the L4 stage

855   (time 0) Scale bar 10 μm. Yellow arrows indicate intact axons with abnormal morphology (axon

856   thinning). White arrow indicates a broken and regenerating axon.

857   (B) Quantification of the fraction of axons with abnormal morphology after 24 hours of β-spectrin

858   degradation from L4 stage to day 1 of adulthood. (unpaired two-tailed t-test: p<0.0001). The

859   number of animals scored is shown above each bar.

860   (C) Quantification of the fraction of axons intact, broken and regenerating, broken and non-

861   regenerating (stump) when β-spectrin is degraded for 24 or 48 hours from L4 stage to day 1 and

862   2 of adulthood. (Fisher's exact test: p<0.0001). The number of animals scored is shown inside

863   each bar.

864

A

B

865
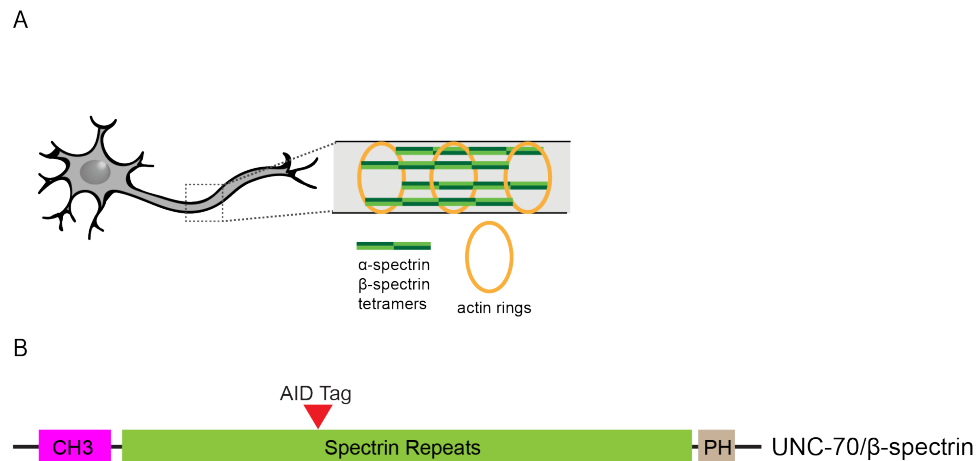
Figure S1: Schematic of the MPS and protein domain structure of *C. elegans* UNC-70/β-spectrin

(A) Cartoon of the MPS comprised of α-spectrin and β-spectrin tetramers linking actin rings

(B) Schematic of the protein domain structure of UNC-70/β-spectrin and location of the AID tag
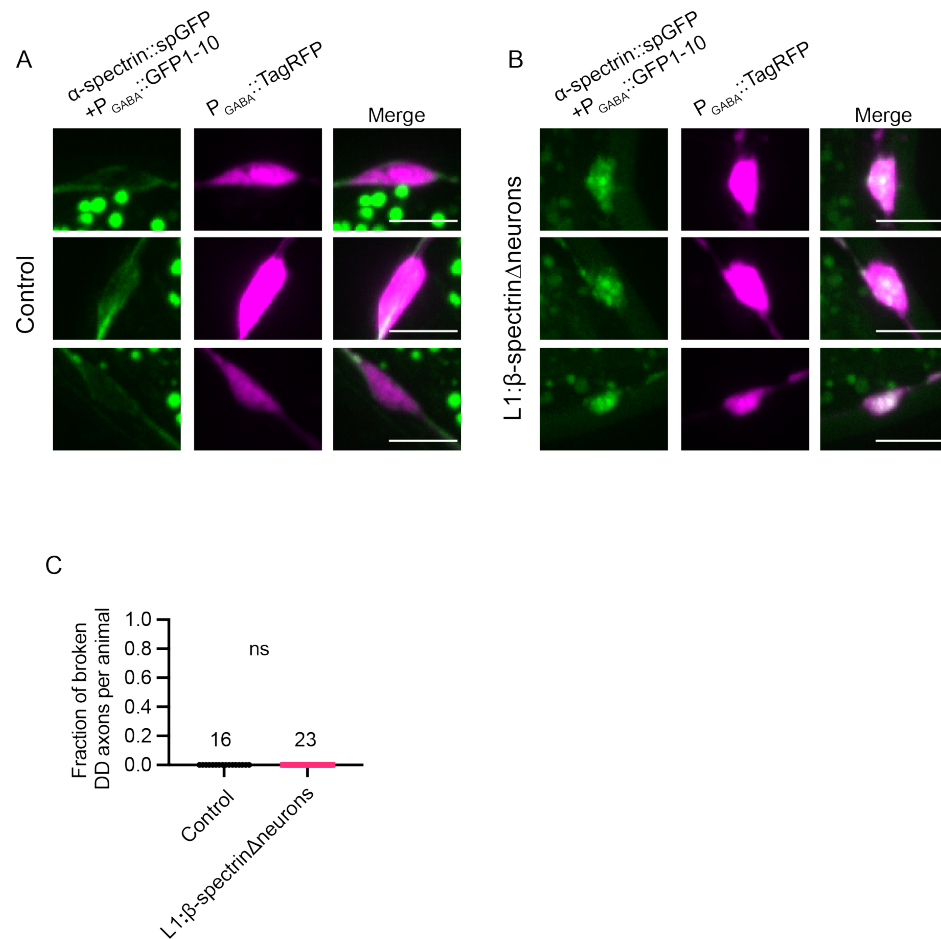
Figure S2: Degradation of neuronal β-spectrin for 24 hours results in accumulation of α-spectrin in DD cell bodies but unbroken DD commissures at the L1 stage

Representative images of endogenous α-spectrin (split-GFP) in DD cell bodies (TagRFP) in (A) control and (B) L1:β-spectrinΔneurons 24 hours after egg lay reveals accumulation of α-spectrin in cell bodies when the MPS is disrupted by degradation of neuronal UNC-70/β-spectrin. Scale bar 5μm.

(C) Quantification of the fraction of broken DD axons 24 hours post egg-lay onto control plates or 1mM auxin (L1:β-spectrinΔneurons). The number of animals scored is shown above each dataset. All animals had 5 visible and intact DD commissures.
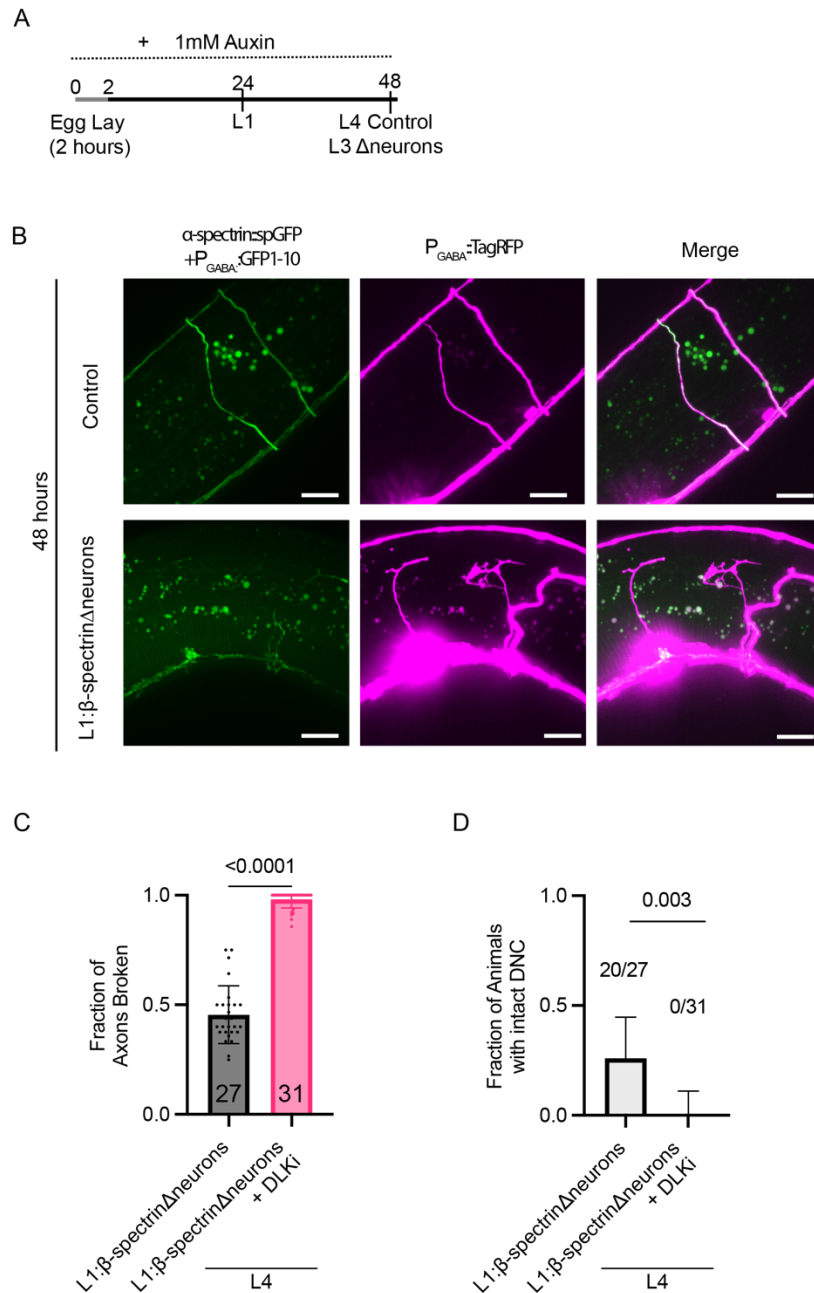
Figure S3: Axons break and regenerate when neurons lack β-spectrin

(A) Schematic of degradation timing for L1:β-spectrinΔneurons assayed at the 48 hour time point. At this timepoint, control animals are L4 stage while L1:β-spectrinΔneurons are slightly developmentally delayed (late L3/early L4)

885   (B) Representative images of endogenous α-spectrin in GABA neurons (split-GFP labeled) and

886   GABA neuron morphology (cytosolic TagRFP) in L4 control and L3/L4 L1:β-spectrinΔneurons

887   animals exposed to 1mM Auxin for 48 hours. Scale bar 10 μm. Extensive growth cone formation

888   is evident in L1:β-spectrinΔneurons animals.

889   (C) Quantification of the fraction of axons broken per animal in L4 stage L1:β-spectrinΔneurons

890   animals with and without inhibition of DLK-1 (DLKi, 50μM GNE-3511) (unpaired two-tailed t-test:

891   p<0.0001).

892   (D) Quantification of the fraction of animals with an intact dorsal nerve cord (DNC) in L4 stage

893   L1:β-spectrinΔneurons animals with and without DLKi (Fisher's exact test: p<0.0001).

894

A
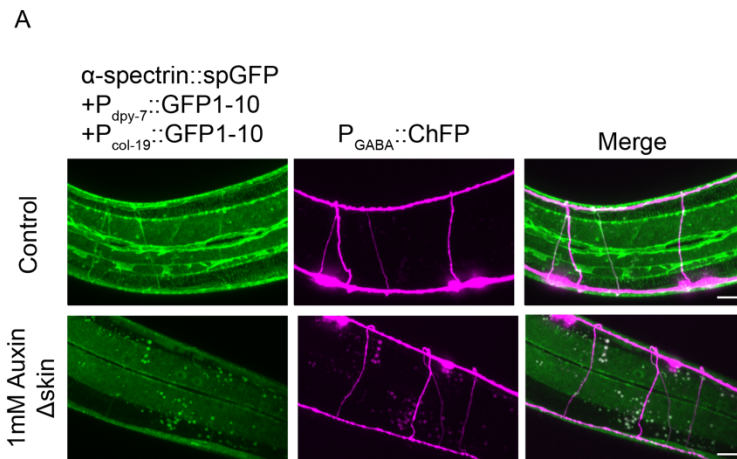
Figure S4: Degradation of epidermal β-spectrin successfully disrupts epidermal α-spectrin

Representative images of endogenous epidermal α-spectrin in control and L1:β-spectrinΔskin
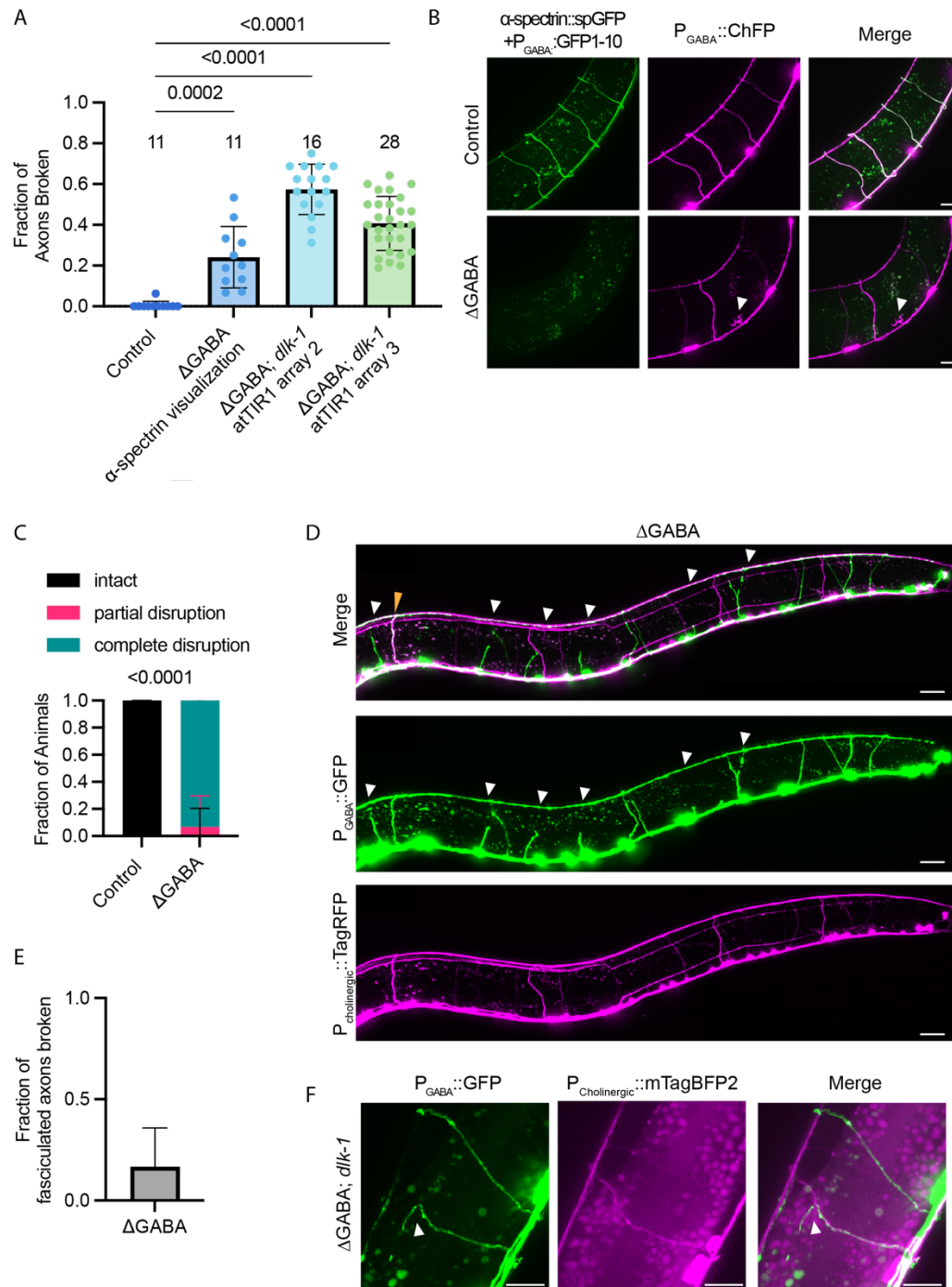
animals at L4 stage. Scale bar 10μm.

900

Figure S5: Neither variability of atTIR1 array nor direct scaffolding by cholinergic neuron

commissures are responsible for the reduced breakage in L1:β-spectrinΔGABA animals

(A) Quantification of the fraction of axons broken in three additional array lines driving atTIR1 in

GABA neurons under the *unc-47* promoter. The dataset labeled ΔGABA α-spectrin visualization

905   is shown in panel B. Arrays 2 and 3 are in the *dlk-1* (j*u476*) background to prevent axon

906   regeneration. (One-way ANOVA followed by Tukey's multiple comparisons test p<0.0001).

907   (B-C) Representative images and quantification of α-spectrin distribution in GABA neurons

908   when β-spectrin is degraded from GABA neurons only. White arrow indicates broken axon.

909   Scale bar 10μm. (Fisher's exact test: p<0.0001).

910   (D) Representative images of cholinergic ($P_{unc-17}::TagRFP$) and GABAergic ($P_{unc-47}::GFP$)

911   neuronal commissures when β-spectrin is degraded from GABA neurons reveals scaffolding

912   from neighboring cholinergic neurons is not common (only 1-2 events per animal). White arrows

913   indicate broken VD/DD GABA axons. Yellow arrow indicates intact GABA commissure

914   fasciculated with cholinergic neuron commissure. This fasciculation event occurs in most

915   animals, and this axon has not been observed to break. Scale bar 20 μm

916   (E) Quantification of the fraction of fasciculation events in which the VD/DD commissure is

917   broken (4/24 broken).

918   (F) Representative images of cholinergic ($P_{unc-17}::mTagBFP2$) and GABAergic ($P_{unc-47}::GFP$)

919   neuronal commissures when β-spectrin is degraded from GABA neurons in the *dlk-1*

920   background reveals fasciculation is not sufficient to prevent breakage. White arrow indicates

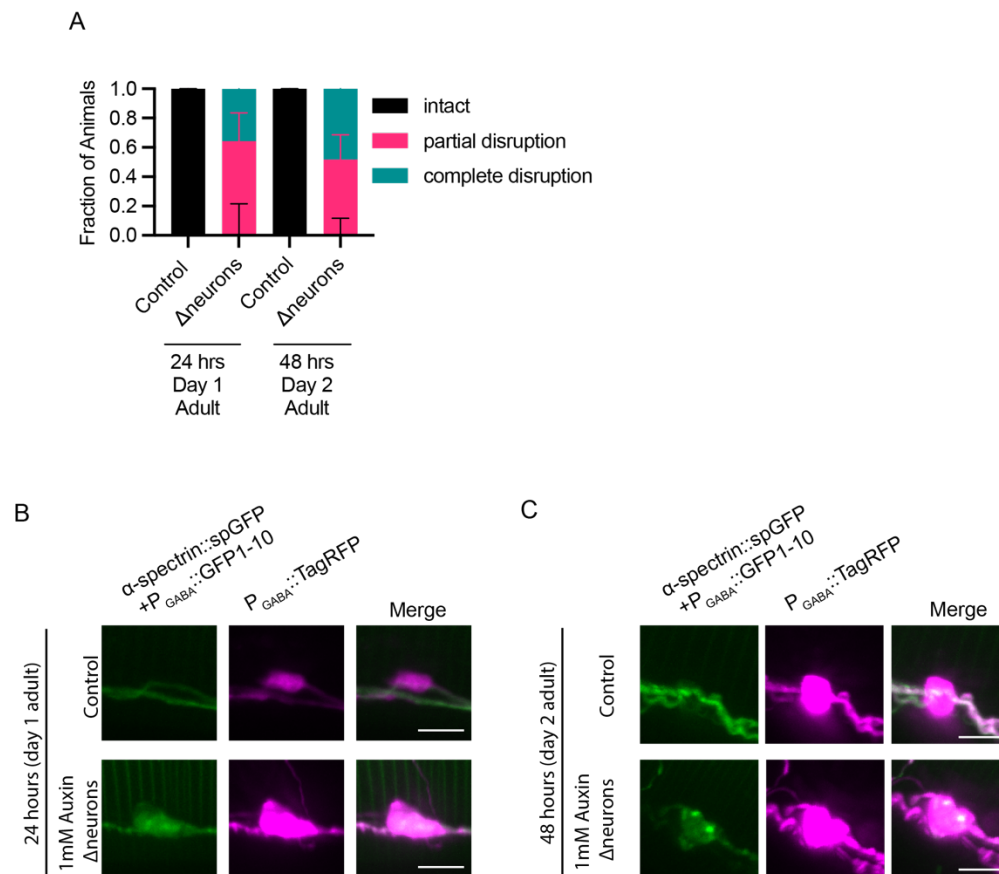921   broken VD/DD commissure. Scale bar 10 μm.

51

922

Figure S6: Degradation of β-spectrin in mature neurons disrupts the MPS

(A) Quantification of the fraction of animals with altered α-spectrin distribution in GABA neurons

when neuronal β-spectrin is degraded for 24 or 48 hours starting at the L4 stage. Complete

disruption of α-spectrin is defined as full loss of endogenous *spc-1* split-GFP signal in GABA

neuron commissures. Partial disruption is defined as some split-GFP signal remaining in one or

more commissures in the worm, but the signal is non-uniform.

(B-C) Representative images of accumulation of α-spectrin (split GFP) in VD/DD cell bodies

(magenta cytosolic TagRFP) upon neuronal β-spectrin degradation for 24 or 48 hours starting at

the L4 stage. Scale bar 5 μm.

932

933

934 **Table S1: List of *C. elegans* strains used in this study**

Strain ID	Genotype	Source	Note	Figure
XE3230	*unc-70(syb1684[unc-70(1166R+AID+1167D)]) V; wpIs495[Prab-3::atTIR1::let-858UTR+Pmyo-2::GFP] IV; oxIs12[Punc-47:GFP, lin-15+] X*	This Study	β-spectrin Δneurons	1, 3
XE3303	*unc-70(syb1684[unc-70(1166R+AID+1167D)]) V; wpIs495[Prab-3::atTIR1::let-858UTR+Pmyo-2::GFP] IV; oxIs12[Punc-47:GFP, lin-15+] X; dlk-1(ju476) I*	This Study	β-spectrin Δneurons; *dlk-1*	3
XE3307	*unc-70(syb1684[unc-70(1166R+AID+1167D)]) V; reSi2[Pcol-10::TIR1::F2A::mTagBFP2::AID*::NLS::tbb-2 3'UTR] II; oxIs12[Punc-47:GFP, lin-15+] X*	This Study	β-spectrin Δskin	4A-C
XE3367	*unc-70(syb1684[unc-70(1166R+AID+1167D)]) V; oxIs12[Punc-47:GFP, lin-15+] X; dlk-1(ju476) I; wpEx562[Punc-47::atTIR1::mRuby::let-858UTR + Pmyo-2::mCherry]*	This Study	β-spectrin ΔGABA; *dlk-1*	S5A array #2
XE3368	*unc-70(syb1684unc-70(1166R+AID+1167D)]) V; oxIs12[Punc-47:GFP, lin-15+] X; dlk-1(ju476) I; wpEx563[Punc-47::atTIR1::mRuby::let-858UTR + Pmyo-2::mCherry]*	This Study	β-spectrin ΔGABA; *dlk-1*	5A-D
XE3449	*wpEx570[Pdpy-7::atTIR1 + Pcol-19::atTIR1 + Pdpy-7::GFP1-10 + Pcol-19::GFP1-10] ; unc-70(syb1684[unc-70(1166R+AID+1167D)]) V; spc-1(cas1047[spc-1::7×gfp11 knock in]) X; vdSi17[Punc-25::ChFP] IV*	This Study	β-spectrin Δskin + α-spectrin:: spGFP_{skin}	4D-F, S4
XE3450	*wpEx571[Punc-47::GFP1-10 + Punc-47::TagRFP]; unc-70(syb1684[unc-70(1166R+AID+1167D)]) V; spc-1(cas1047[spc-1::7×gfp11 knock in]) X; wpIs495[Prab-3::atTIR1::let-858UTR+Pmyo-2::GFP] IV*	This Study	β-spectrin Δneurons + α-spectrin:: spGFP_{GABA}	2, S2, S3, 6, S6

53

XE3461	*wpEx573[Punc-47::atTIR1::mRuby:: let-858UTR + Punc-17::mTagBFP2 + Pmyo-2::mCherry]; unc-70(syb1684[unc-70(1166R+AID+1167D)]) V; oxIs12[Punc-47::GFP, lin-15+] X; dlk-1(ju476) I*	This Study	β-spectrin ΔGABA; *dlk-1* + Pcholinergic:: mTagBFP2	S5A,F, array #3
XE3462	*wpEx574[Punc-47::atTIR1::mRuby:: let-858UTR + Punc-17::atTIR1::let-858UTR + Punc-17::mTagBFP2 + Pmyo-2::mCherry]; unc-70(syb1684[unc-70(1166R+AID+1167D)]) V; oxIs12[Punc-47::GFP, lin-15+] X; dlk-1(ju476) I*	This Study	β-spectrin ΔGABA Δcholinergic; *dlk-1*	5B-D
XE3463	*wpEx575[Punc-47::atTIR1::mRuby:: let-858UTR + Pdpy-7::atTIR1::tbb-2UTR + Pcol-19::atTIR1::let-858UTR+ Punc-17::mTagBFP2 + Pmyo-2::mCherry]; unc-70(syb1684[unc-70(1166R+AID+1167D)]) V; oxIs12[Punc-47:GFP, lin-15+] X; dlk-1(ju476) I*	This Study	β-spectrin ΔGABA, Δskin; *dlk-1*	5B-D
XE3465	*wpEx577[Punc-47::atTIR1::mRuby::let-858UTR + Punc-47::GFP1-10::let-858UTR + Pmyo-2::mCherry]; unc-70(syb1684[unc-70(1166R+AID+1167D)]) V; spc-1(cas1047[spc-1::7×gfp11 knock in]) X; vdSi17[Punc-25::ChFP] IV*	This Study	β-spectrin ΔGABA + αspectrin:: spGFP$_{GABA}$	S5A,B
XE3485	*wpEx590[Punc-47::atTIR1::mRuby::let-858UTR + Punc-17::TagRFP::let-858UTR + Pmyo-2::mCherry]; unc-70(syb1684[unc-70(1166R+AID+1167D)]) V; oxIs12[Punc-47::GFP, lin-15+] X*	This Study	β-spectrin ΔGABA; + cholinergic:: TagRFP	S5D,E

935

936

54

937 **Table S2: List of plasmids used in this study**

Plasmid identifier	Description	Concentration Injected (ng/uL)
pHHW-004	Prab-3::atTIR1::let-858UTR	20
pPD118.33	Pmyo-2::GFP	5
pSEM319	Fragment of unc-119 MoSTI site Addgene: #159823	5
pCFJ90	Pmyo-2::mCherry	1
pCAD145	Punc-47::atTIR1::mRuby::let-858UTR	20
pCAD165	Pdpy-7::atTIR1::tbb-2UTR	20
pCAD154	Pcol-19::atTIR1::let-858UTR	20
pCAD164	Pdpy-7::GFP1-10::tbb-2UTR	20
pCAD163	Pcol-19::GFP1-10::tbb-2UTR	20
pCAD136	Punc-47::GFP1-10::let-858UTR	20
pCAD169	Punc-47::TagRFP::let-858UTR	20
pCAD174	Punc-17::mTagBFP2::let-858UTR	20
pCAD170	Punc-17::atTIR1::let-858UTR	20
pCAD179	Punc-17::TagRFP::let-858UTR	30

938